A THESIS

On

Synthesis and characterization of doped nano-phosphor for luminescence studies

Submitted in the partial fulfillment of requirement for award the degree of

M. Tech. (Materials & Metallurgical Engineering)

Under supervision:

Dr. K.K. Raina
Deputy Director & Dist. Professor
SPMS

Work carried out at:

Global R&D AMPTC, Crompton Greaves Ltd., Mumbai

Submitted by:

Pankaj Chamoli
Roll .no. 600802012
School of Physics and Materials Science
Thapar University
Patiala, Punjab

JULY, 2010

Dedicated

To

My Father

(1958-1987)

Laid his life in Operation" Pawan" Sri Lanka

CERTIFICATE

This is to certify that the thesis entitled ***"Synthesis and characterization of doped nano-phosphor for luminescence studies"*** *submitted by* ***Mr. Pankaj chamoli*** *in the partial fulfillment of the requirement for the award of the degree of* ***M.Tech.*** *in* ***Material Sci.& Metallurgical Eng.*** *from the* ***School of Physics and Material Science, Thapar university, Patiala, Punjab****, is a record of candidate's own work carried out by him under my supervision and guidance. The matter embodied in this report has not been submitted in the part of full to any other university or institute for the award of any degree.*

(Dr. K.K. Raina)
Deputy Director & Dist. Professor
SPMS, Thapar University
Patiala, Punjab

Countersigned by:

(Dr. O.P. Pandey)
Professor & Head
Thapar university
Patiala

Dated :

(Dr. R.K. Sharma)
Dean, Academic Affairs
Thapar university
Patiala

Dated:

CERTIFICATE

This is to certify that the thesis entitled ***"Synthesis and characterization of Doped nano-phosphor for luminescence studies"*** *submitted by* ***Mr. Pankaj chamoli*** *in the partial fulfillment of the requirement for the award of the degree of* ***M.Tech.*** *In* ***Materials sci.& Metallurgical Eng.*** *from the* ***School of Physics and Material Science, Thapar university, Patiala, Punjab****, is a record of candidate's own work carried out by him under my supervision and guidance. The matter embodied in this report has not been submitted in the part of full to any other university or institute for the award of any degree.*

(Dr. K.K. Raina)
Deputy Director & Dist. Professor
SPMS, Thapar University
Patiala, Punjab
Dated:

(Mr. Lokesh Chaudhari)
Sr. Executive Technology
Global R&D Centre
AMPTC, CG Ltd.
Mumbai

Acknowledgement

This thesis is the result of many long hour involving arduous research and the culmination of a process that included the constant assistance, support & guidance afforded to me by my fellow academician and professionals whom I am deeply indebted. This achievement been accomplished, in no small measure, due to their sheer professionalism and dedication which they demonstrated time after. It is to them that I owe my heartfelt thanks and the overwhelming sense of satisfaction that I feel at this stage.

A special thank you to Dr. K.K.Raina my supervisor who greatly enriched my knowledge & constantly inspired me and gave me a chance to do work in Mumbai. He has been able to skillfully manage this research without forgetting the ever essential human relationships.

I am thankful to Dr. Vivek Singal, Head, Global R&D AMPTC, Crompton Greaves Ltd., Mumbai, for providing the Practical support in allowing, me use of their Laboratories & facility. My overwhelming thanks go to Dr. R. Shankar and Dr. Rajendra Jeswal for his encouragement and support especially on the practical ground and moral support during the completion of this research work and for providing all possible laboratory facility to carry out the experimentation.

I would like to offer my heartfelt thanks to Dr. K.V.N.R. Murthy, Reader, Material Display Laboratory, M.S.University, Baroda, for giving permission to carried out my PL characterization in Material Display Laboratory, M.S.University, Baroda.

I would like to thank all those members of the Global R & D AMPTC, Crompton Greaves Ltd., Mumbai, who have contributed to make my stay very pleasant. I am particularly thankful to Dr. Asha Ingle, Mr.Lokesh choudhari , Dr. Pradeep Roy , Dr. David Dimelo, Mr. T. Rakesh, Mr. Sharwana , Mr.Sushil, Mis. Jaishri for their invaluable help and friendliness. I am indebted to the fellow students in Global R&D, C G Mr. Naveen , Mr. Rajpal, Mr. Jetaindar for their support and Encouragement.

I would like to offer my heartfelt thanks to Dr. O.P. Pandey, Head, SPMS, Thapar University, for giving permission to carried out my work in Crompton Greave Global R&D, Mumbai.

I also thank full to research scholar Ms. Sikha Kapila, Mr. Ravi Sukla, Ms. Neeraz Sharma, Materials Research Lab, Thapar University, Patiala, for their Moral support and Guidance.

A special mention to my Mom who through thick & thin always there for me and never doubted my ability.

I am also thank full to my friends Mr. Ishan choudahry, Mr. Sumit Bhardwaj, Mr. Anil, Ms. Sunita Mehta, Ms. Poonam Sharma and all the staff member of SPMS, Thapar university for their full cooperation, motivation and generous support. My greatest thanks are due to all wished me success. .

All these thanks are however only fraction of what is due to Ambiguity for granting me an opportunity and strength to successfully accomplish his assignment.

Pankaj Chamoli

Abstract

Present study is an attempt to synthesize pure, Mg and Mn doped ZnO via solid state reaction method and chemical co-precipitation route using various solvents in basic medium. The structural morphological, chemical and optical properties were studied by using X-Ray diffraction, Scanning electron microscopy, Fourier transform infrared spectroscopy, UV-VIS and Photoluminescence spectrophotometer. XRD analysis inferred that the pure and doped sample prepared by SSR method and chemical approach (ethanol and methanol) were single phase and exhibited wurtzite hexagonal structure up to the higher dopant concentration(15%). However, the samples prepared in the presence of distilled water accept the dopant only up to 7%. Well defined spherical grains were noticed in the sample prepared by SSR, however, no definite morphology has been observed in the samples derived via chemical route. Chemical study gives only the preliminary signatures of the ZnO phase formation. The band gap observed for the chemically synthesized samples was found to increase with the increment in the dopant concentration. Violet and blue emissions have been noticed for all the samples when excited at the wavelength 250 nm.

TABLE OF CONTENTS

LIST OF FIGURES

LIST OF TABLES

Chapter 1
Introduction and literature review

1.1Nano science and Technology

1.1.1 Introduction of Nanotechnology

The term nanotechnology has evolved over the years via terminology drift to mean, ”Anything smaller the micro technology”. Such as Nano powder and other things that are nanoscale in size. The Greek word ‘Nano’ referred to the length scale of one billionth of meter. Thus nanoscince deal with the science of materials and technologies in the scale range of 1-100 nm. This means, the nanoscience deals with a few hundred to a few thousand atoms or atomic clusters, whereas the microscopic word is made out of trillion of atoms or molecules .Nanopartilces are larger than individual atom and molecules, but are smaller than bulk solid :hence they obey neither absolute quantum chemistry nor laws of classical physics and have properties that differ markedly from these expected.

Presently the nanoscience and technology represents the most active disciple all around the world and is considered as the fastest growing technology revolution in the human history had ever seen. This intense interest in the science of the materials confined within the atomic scales seems the fact that these nonmaterial’s exhibit fundamentally unique properties with great potential of bringing plethora of nest generation technologies in electronics, computing, optics, biotechnology, medical imaging medicine ,drug delivery ,structural materials ,aerospace ,energy etc. Recently the Foresight institute has suggested as alternate thing to represent the original meaning of nano technology: Zettatechnology [1]

1.1.2 Nanostructure materials

Synthesis of nanopaticles (Zero, one, two and three-dimensional) has become a focal area in nanostructure materials research owing to their low dimensions characteristics which differ from the bulk [2]. Nonmaterial’s are increasingly gaining the attention of not only the scientific community but also the public due to their unique properties, which lead to new and exciting application. The physical and chemical properties of the nanomaterial’s tend to be exceptionally closely dependent on the size and shape or morphology. It is interesting to note that by changing the preparation parameter. Nanomaterial’s having wide range baring

morphology such as spherical Nanoparticals, Nanowires, Nanoroads and Nanotubes can be synthesized.[3-5]

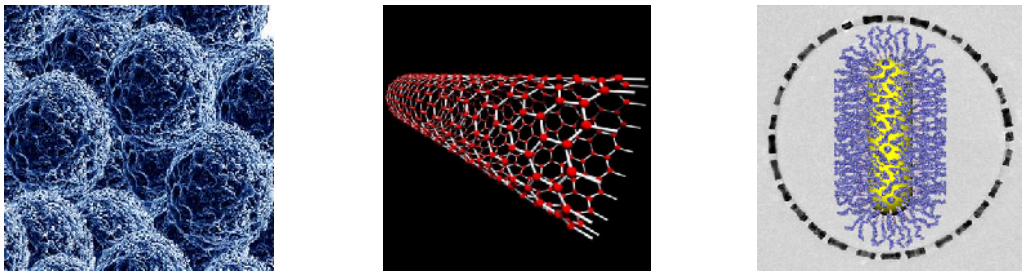

Fig 1.1. (a) Nanomatrials (b) Nanotube (c) Nanorod

1.1.3 Semiconducting Nano-particles

Michael Faraday provided the first description, in scientific terms, of the optical properties of nanometer-scale metals in his classic 1857 paper. In a subsequent paper, the author (Turner) points out that: "It is well known that when thin leaves of gold or silver are mounted upon glass and heated to a temperature which is well below a red heat (~500 °C), a remarkable change of properties takes place, whereby the continuity of the metallic film is destroyed. The result is that white light is now freely transmitted, reflection is correspondingly diminished, while the electrical resistivity is enormously increased."[6-8].Almost all materials system including metal insulators and semiconductors show size dependent electronics or optical properties in the quantum size regime. Among these, the modification in the energy band gap of semiconductors is the most attractive one because of the fundamental as well as technological importance. Semiconductors with widely tunable energy band gap are considered to be the materials for next generation flat panel displays ,photovoltaic ,optoelectronics devices laser, sensors, phonic band gap devices etc.

When dimension of a materials is continuously reduced from macroscopic size to nanometer , the physical and chemical properties drastically change. If one dimension is reduced to nanometer range, so that the size is comparable to the de-Broglie wavelength of the exciton ; while other two dimensions remains large, one obtains a structure known as quantum well. If two dimension are reduced and one remains large the resulting structure is referred as quantum wire .And if all there dimension are reduced the materials is called a quantum dot. The word quantum associated with these three types of the nanostructures because the change

in properties arise for quantum mechanical nature of physics in ultra small domain. In quantum dots, the surface to volume ratio is large and surface effects dominate.

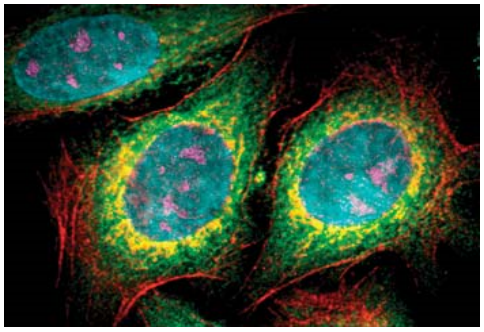

Fig1.2. Quantum Dot

1.1.4 Properties of Nano-materials

The various material properties such as electrical, mechanical, optical, magnetic etc are highly influenced by the fine grained structure and there is generally improvement is the concerned properties. Using a Varity of synthesis methods ,its is possible to produce nanostructure materials in the various forms like: thin films ,powder, quantum wires, quantum wells quantum dots etc. there is also considerable interest in the generation of carbon nanostructure, which are related the famous Bucky ball. In addition, the use of nano sized materials as fillers for composite materials are generating interest; specially in the case of polymer nano composites. All materials are generating interest; specially in the case of polymers nano composites, composed of grains. These grains are usually invisible to the naked eye, depending on the size .Conventional materials have grains braying in size any where form 100's of microns to millimeters [9]

1.2 Overview of Zinc Oxide

Zinc oxide (ZnO), a II-VI direct wide band gap semiconductor, has been studied by the scientific community since the 1930s [10]. Although it has unique and interesting properties, such as a relatively high exciton binding energy (60 meV), and a wide band gap (3.3 eV), and is piezoelectric, biologically safe and biocompatible [11], researchers' work with ZnO has previously been focused on obtaining stable p-type dopants for ZnO. In addition to these excellent properties, ZnO possesses a large number of extrinsic and intrinsic deep-level

impurities and complexes (clusters) that emit light of different colors , including violet, blue, green, yellow, orange and red, all constituents of white light [11][12][13].

Because of this, ZnO is considered to be attractive for applications requiring luminescent materials. ZnO, especially in its nanostructure form, is currently attracting intense global interest for photonic applications. ZnO has the additional advantages of being easy to grow and possessing the richest known family of nanostructures [14]. The present global interest in ZnO nanostructures is motivated by the possibility of growing them on any p-type substrate and hence producing high quality p-n heterojunctions. The interest in optoelectronic applications arises from the possibility of developing low energy and environmentally friendly white light emitting technologies and laser diodes that operate above room temperature.

The renewed interest in utilizing the excellent properties of ZnO in optoelectronic devices is mainly due to the ZnO ambipolar doping problem mentioned above. This problem frequently occurs in wideband gap materials, in which it is very easy to dope the material with one polarity but is very difficult to dope the same material with the other polarity. As ZnO is naturally n-type, it is very difficult to dope it with materials of p-type polarity [15]. Several laboratories have reported p-type ZnO, but their results were difficult to reproduce in other laboratories and hence remain controversial. Elements from group I, including Li, Na, and K, as well as elements like Cu and Ag, are supposed to be good acceptors when replacing a Zn site, and they form deep acceptors with ionization energies around a few hundred meV above the valence band [16]. This implies that at equilibrium, doping can be achieved without any ionization leading to free holes. Moreover, at high levels of doping with such elements, interstitial Li (or Ag) atoms will act as donors and compensate many acceptors [17][18].
Another possibility for doping ZnO to p-type is to use elements from group V on the O site, including N, P, Sb, and As. Most efforts to use these elements have led to poorly reproducible results. An elegant summary of all of these efforts is documented in Look et al. [19]. Most recently, there have been successful reports of doping ZnO with N, forming a level with ionization energy of around 100 meV, less than the 160 meV ionization energy of the standard Mg acceptor in GaN [15].Due to the existence of other native deep levels close to the conduction band, the compensation effect makes these efforts unsuccessful in producing stable and highly doped p-type ZnO materials. The difficulty in doping ZnO to p-type polarity has led researchers to seek to create hetero junctions with other p-type semiconductor

materials to enable ZnO to be used in optoelectronic devices. These efforts began by growing n-type ZnO thin films on p-type substrates. However, due to lattice mismatches, most of these efforts have noted to the development of device-quality heterojunctions.

Table1.1 Basic physical properties of ZnO

Property	**Value**
Lattice parameter at 300 K (a)	3.2495 A^0
Lattice height at 300 K (c)	5.2069 A^0
c/a ratio	1.602
Density	5.606 g-cm^{-3}
Stable phase at 300 K	Wurtzite
Bond length	1.977 μm
Melting point	1975^0C
Thermal conductivity	0.6 , 1-1.2
Static dielectric constant	8.656
Refractive index	2.008, 2.029
Energy gap	3.4 eV, direct
Exciton binding energy	60 MeV
Iconicity	62%
Heat capacity Cp	9.6cal/mol K
Young's modulus E (Bulk ZnO)	111.2±4.7 Gpa

The efforts in growing thin films of n-type ZnO on different p-type substrates, along with many of the fundamental properties of ZnO, are described in the comprehensive review written by Özgur et al.[20]. Nano-structures, especially nanorods or nanowires, possess a relatively large surface area to volume ratio, enabling them to release stress and strain due to

lattice mismatch with other materials. In addition, ZnO has been shown to be able to produce a rich family of different nanostructures; as a wurtzite structure, ZnO has a total of 13 different facet growth directions: <0 0 0 1>, <0 1 −1 0>, <2−1 −1 0>. Together with a pair of polar surfaces {0001}, this uniquely structured material has been demonstrated to form a diverse group of nanostructures: nanorods, nanobelts, nanocombs, nanosprings, nanorings, nanobows, nanojunction arrays, and nanopropeller arrays, which are formed largely due to the highly ionic character of the polar surfaces [21]. Some ZnO nanostructures (namely tetrapods) were unintentionally synthesized as early as 1944. At that time, there were no microscopes with sufficient resolution to view the synthesized structures, which have since been identified as tetrapods [22].

The different growth methods used to obtain ZnO nanostructures can be divided into two main groups: low (<100 °C) and high (up to 1000 °C) temperature techniques. High quality ZnO nanostructures have been grown on a variety of crystalline as well as amorphous (polymer) substrates and formed excellent p-n heterojunctions, in contrast to thin films of ZnO, which have shown very limited success in forming heterojunctions. One advantage of n-ZnO nanorods on any p-substrate is that each nanorod will form a discrete, separated p-n junction, and hence a large-area light emitting diode can be designed without compromising the junction area, which would lead to large reverse leakage currents. This is an important property that is advantageous for large-area lighting commercialization.

1.3 Structural properties of Zinc Oxide

1.3.1Crystal structure and Growth directions

Being a wurtzite-structured oxide with lattice parameters a=0.3296nm and c=0.52065 nm,. ZnO can be simply described as a number of alternating planes composed of tetrahedrally coordinated O^{2-} and Zn^{2+} ions, stacked alternately along the c-axis.The strongest polarity occurs along c-axis with positively charged Zn^{-}(0001) polar surface and negative charged O^{-} (000-1) polar surface. Wurtzite-structured ZnO has a total of 13 different facet growth directions: <0 0 0 1>, <0 1 −1 0>, <2−1 −1 0>. Together with a pair of polar surfaces {0001}[21] and three set of lowest energy surfaces within the crystal, {0001}, {01 1 0}, and {2 1 1 0}, and three fast growth directions, [0001], [01 1 0], and [2 1 1 0]. Four possible nanobelt are the most common ZnO nanobelts observed experiments, although nanobelts grown along other directions are also possible. Among all growth directions, [0001] direction

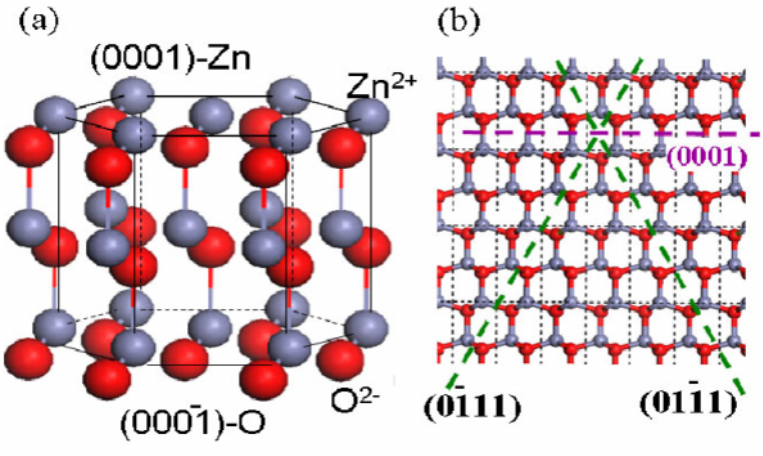

Fig1.3. Schematic representations of the ZnO wurtzite crystal structure [23]

is the fastest growth direction among Wurtzite crystal. As a result, ZnO nanobelt grown along [0001] with the No 1 configuration in Fig.1.4 are commonly observed in different synthesis experiment. This kind nanobelt has non-polar surfaces as its side surfaces. No 2 configuration has a growth direction of [01 1 0] and polar ± (0001) surface as its smaller side surfaces. A stacking fault along the whole length is always observed in this kind of nanobelt, which can reduce the barrier to growth. In comparison, No 3 and No 4 configuration have a growth direction along [01 1 0] and [2 1 10] respectively and have polar ± (0001) surfaces as their primary (larger) side surfaces. Thus, these nanobelts in no. 3 and no. 4 configuration are also defined as polar-surface dominated (PSD) nanobelts. Based on their geometry and crystallographic orientation, polar-surface-dominated nanobelts have induced a great variety of novel nanostructures.

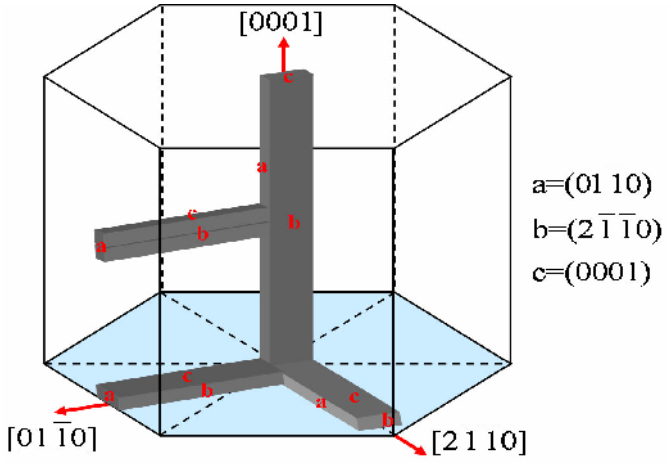

Fig1.4. Growth direction in Zinc Oxide

1.3.2 Band structure

This is the most important property of semiconductor since it is responsible for the wide range of electrical properties observed in material [24] and determine the potential application of the material [25].in any semiconductor material ,this structure is such that the filled valance band is separated from an empty conduction band by a band gap containing no allowed energy state at 0K[24].a number of theoretical approaches using different degree of complexity and also several experiments have been carried out to calculate the band structure and electronic state of the wurtzite structure of ZnO, respectively[25].The E-K diagram is showing in Fig1.5.

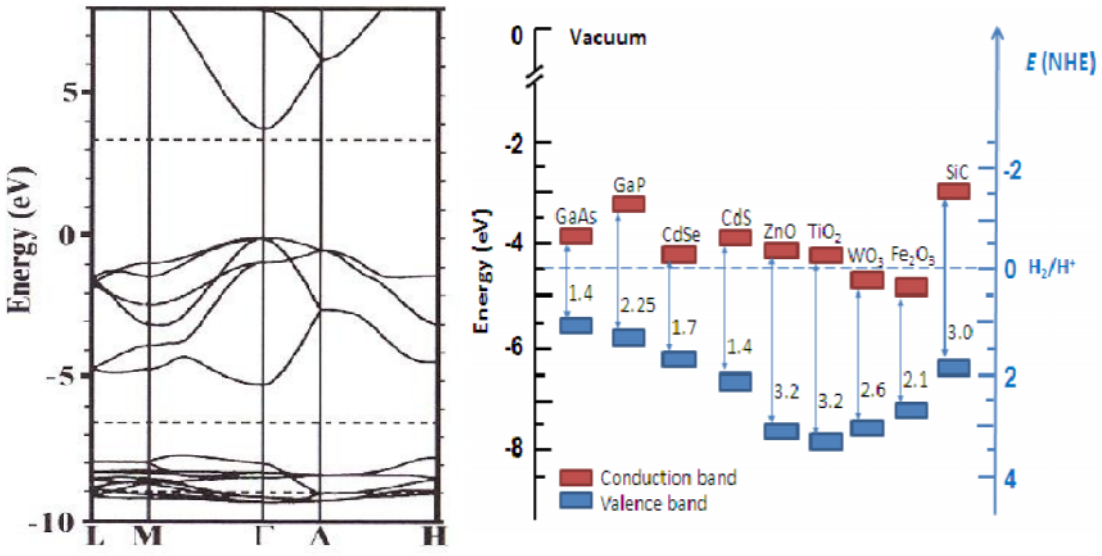

Fig1.5. Energy diagrams for various semiconductors in aqueous electrolytes at pH= 1[26]

1.4 Electrical properties

ZnO has a relatively large direct band gap of 3.3 eV at room temperature; therefore, pure ZnO is colorless and transparent. Advantages associated with a large band gap include higher breakdown voltages, ability to sustain large electric fields, lower electronic noise, and high-temperature and high-power operation. The band gap of ZnO can further be tuned from ~3–4 eV by its alloying with magnesium oxide or cadmium oxide.

Most ZnO has *n*-type character, even in the absence of intentional doping. Nonstoichiometry is typically the origin of n-type character, but the subject remains controversial. An alternative explanation has been proposed, based on theoretical calculations, that

unintentional substitutional hydrogen impurities are responsible. Controllable n-type doping is easily achieved by substituting Zn with group-III elements such as Al, Ga, In or by substituting oxygen with group-VII elements chlorine or iodine.Reliable p-type doping of ZnO remains difficult. This problem originates from low solubility of p-type dopants and their compensation by abundant n-type impurities. This problem is observed with GaN and ZnSe. Measurement of p-type in "intrinsically" n-type material is complicated by the inhomogeneity of samples. Current limitations to p-doping do not limit electronic and optoelectronic applications of ZnO, which usually require junctions of n-type and p-type material. Known p-type dopants include group-I elements Li, Na, K; group-V elements N, P and As; as well as copper and silver. However, many of these form deep acceptors and do not produce significant p-type conduction at room temperature. Electron mobility of ZnO strongly varies with temperature and has a maximum of ~2000 $cm^2/(V \cdot s)$ at 80 K. Data on hole mobility are scarce with values in the range 5–30 $cm^2/(V \cdot s)$ [27][28].

1.5 Thermal properties

1.5.1. Thermal expansion coefficient (TEC)

The change in temperature affects the lattice parameters of semiconductors. Thermal expansion coefficient, are defined as or α_a or α_c for in and out of plane cases, respectively. The stichiometry, presence of extended defects and free carrier concentration also affect the thermal expansion coefficient. The X-ray powder diffraction method by Reeber was used to measure the temperature dependence of lattice parameters of ZnO as shown in Figure1. 6**.** Lattice parameters of ZnO were measured over the temperature range 4.2 -299 K, fourth-order polynomials were fitted using the least-squares method, which gives the minimum for the ‘a’ parameter at 93 K. The ‘c’ parameter has much uncertainty, did not give any minimum value, perhaps due to its less precision and uncertainty in measurement [29].

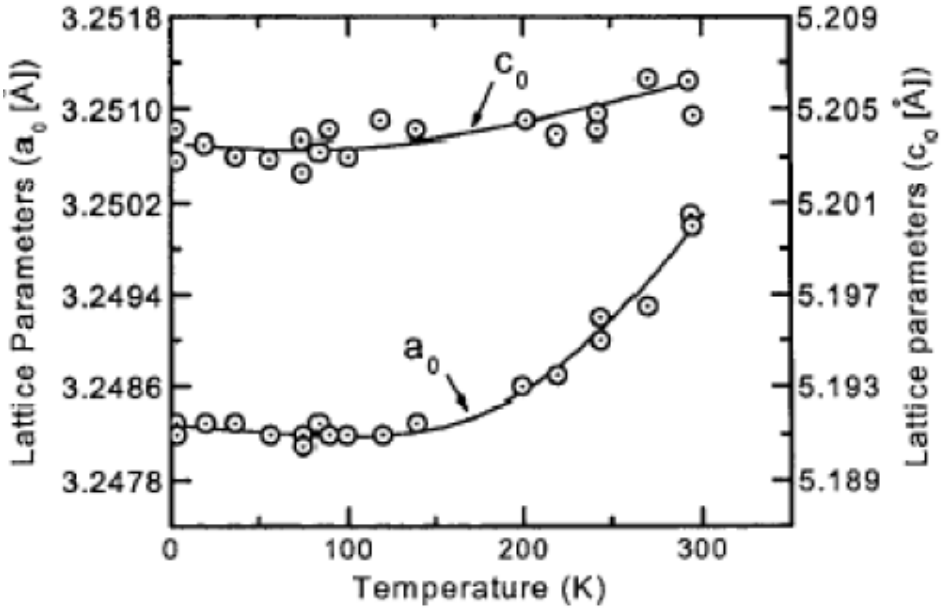

Fig1.6. Wurtzite ZnO lattice parameters as a function of temperature.

1.5.2. Thermal conductivity

Thermal conductivity (k), having a kinetic nature, is determined by vibration, rotation and electronic degree of freedom. It is really important property of semiconductors when these materials are used in high-power, high-temperature or optoelectronic devices. The electronic thermal conductivity is very small, having light carrier concentration, which is negligible.

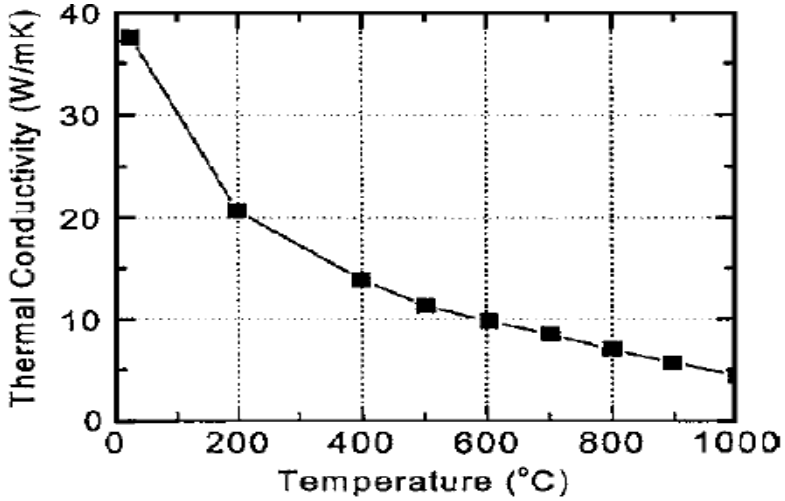

Fig1.7. Thermal conductivity of fully sintered ZnO heated from room temperature to 1000

For high pure crystals, phonon-phonon scattering is ideally proportional toT^{-1} at the temperatures higher than the Debye temperature. Point defects, such as vacancies, impurities and isotope fluctuations in a ZnO affect the thermal conductivity of ZnO material.

The thermal conductivity of fully sintered ZnO at temperatures from room temperature to 1000°C is measured. Fig.1.7 shows the thermal conductivity curve for a fully dense ZnO crystal. The thermal conductivity decreases from 37 to 4 W/m K as the temperature is increased from room temperature to 1000 °C. The dominant scattering mechanism is resistive phonon-phonon interactions [30].

1.6 Optical properties: Zinc Oxide as a phosphor

1.6.1 General features about zinc oxide photoluminescence

ZnO is a direct band semiconductor and a transparent conductive material. ZnO films are transparent in the wavelength range of 0.3 and 2.5 μm, and plasma edge lies between 2 and 4 μm depending on the carrier concentration. It is well known that a shift in the band gap edge appears with an increase in the carrier concentration. This shift is known as Burstein-Moss shift. Optical transitions in ZnO have been studied by a variety of experimental techniques such as optical absorption, transmission, reflection, spectroscopic.Ellipsometry, photoluminescence, cathodoluminescence, calorimetric spectroscopy, etc. Room temperature PL spectrum of ZnO is usually composed of a near UV-emission band (375 nm) and a green emission band (510 nm) although a yellow-orange band (610 nm) can also be observed in some situations.

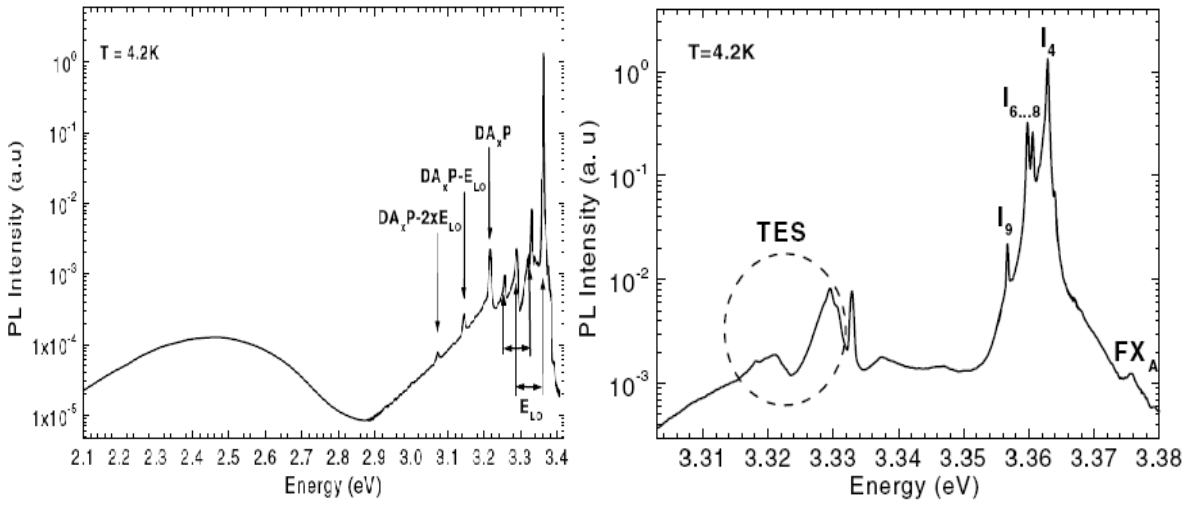

Fig.1. 8. Typical ZnO PL spectra at T = 4K. **(a)** Whole range from 2.1 to 3.4 eV; the DAP peak and some phonon replicas are indicated (see text for details) **(b)** Excitonic range [32]

The near UV-band is closely related to the excitonic nature of the material and may be superposed with the free exciton emission, its phonon replica, bound exciton emission. The observation of luminescence from exciton is usually difficult even at low temperatures. This comes from a lot of factors [31].

1.6.2 Excitonic emission (near band-edge emission)

As told before, zinc oxide is a direct band gap semiconductor crystallizing in the wurtzite crystal structure. The valence band is six-fold degenerate, but the spin-orbit coupling partially removes this degeneracy, splitting one sub-band, and due to the wurtzite crystal structure the crystal field splitting separates the other two sub-bands; therefore the valence band is constituted by the three two-fold degenerate sub-bands, named *A* (heavy hole band), *B* (light hole band) and *C* (crystal-field split band).

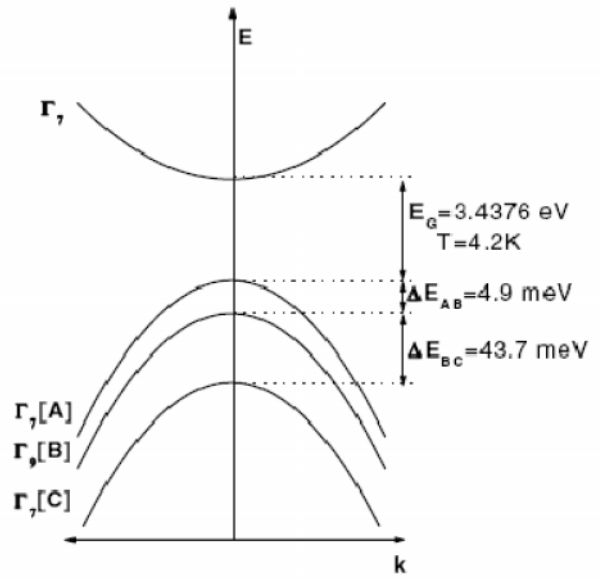

Fig.1.9. Schematic representation of the ZnO band structure near the band-gap.[32]

1.6.3 Luminescent centre in Zinc Oxide

Efficient donors and acceptors have energy levels near the conduction and valence bands, and deep centers also exist with energy levels deep in the forbidden gap. The room temperature photoluminescence (PL) spectrum of ZnO nanorods / nanowires with diameters larger than 20 nm is similar to the PL spectra of bulk ZnO. This room temperature PL spectrum is normally characterized by near-band-edge (NBE) ultra-violet (UV) emission and at least one broad band emission due to deep levels, called DLE. DLE refers to the broad band extending

from just above 400 nm up to 750 nm. The broadness of the band results from the fact that it represents a superposition of many different deep levels emitting at the same time. Different reports have suggested different deep levels as the origin of the observed emissions.

The deep levels of ZnO are divided into extrinsic and intrinsic deep levels. The possible intrinsic 'native' deep levels in ZnO are oxygen vacancy (V_O), zinc vacancy (V_{Zn}), oxygen interstitial (Oi), zinc interstitial (Zni), oxygen anti-site (O_{Zn}), and zinc anti-site (ZnO). This is in addition to native defect clusters, which are usually formed by the combination of two point defects or one point defect and one extrinsic element, e.g., a V_O Zn_i cluster formed by Zni and VO. This V_O Zni cluster is one of the clusters that has been previously identified and is situated 2.16 eV below the conduction band minimum. These native point defects often directly or indirectly control doping, compensation, minority carrier lifetime and luminescence efficiency in semiconductors. Native defects are often invoked to explain the fact that ZnO always exhibits a high level of unintentional n-type conductivity [33]. The concentration of a point defect depends on its formation energy. At thermodynamic equilibrium and in dilute cases (no defect-defect interaction), the concentration of a point defect (c) is given by [33]:

$$c = N_{sites} \exp\left(-\frac{E^f}{k_B T}\right) \qquad \text{.....(1)}$$

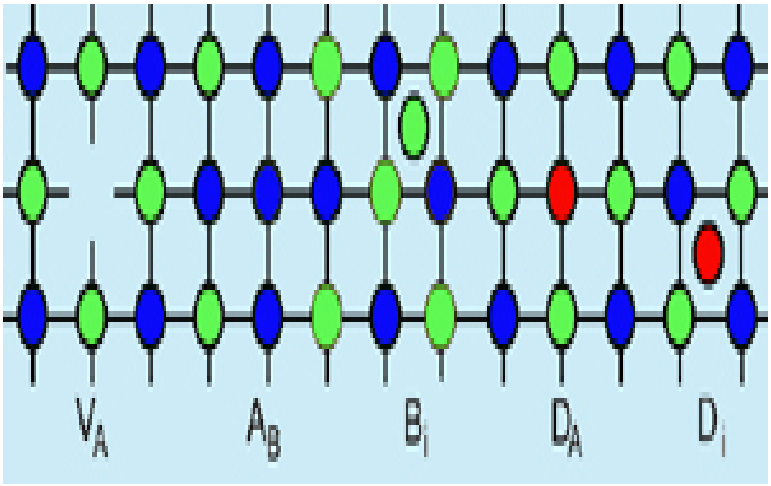

Fig.1.10 Point defect of ZnO [35]

where c is the point defect concentration, E^f is the formation energy, Sites N is the number of available sites to accommodate the defect, kB is Boltzmann's constant, and T represents temperature. According to equation 1, defects with high formation energies will occur at low concentrations. The formation energy E^f of point defects is not constant, but rather depends on the growth parameters and annealing conditions [34].

As discussed above, these deep levels introduce levels in the band gap of the semiconductor that involve transitions between different charge states. The transition levels can be experimentally observed when the final charge state fully relaxes to its equilibrium configuration after the transition, such as in deep level transient spectroscopy (DLTS) [36]. Conventionally, if the transition level is situated such that the defect is most likely to be ionized at room temperature or at the device operating temperature, then this is called a shallow transition level [33]. If the transition level is unlikely to be ionized at room temperature, then it is a deep transition level. The first step in the discussion on deep level native defects in Zn_O is to consider V_O. V_O and Zn_i have long been suggested to be sources of the observed unintentional doping in ZnO, which is due to shallow levels situated 30–40 meV below the conduction band minima [37][38].

Table1.2 Some recently reported lines emitted from ZnO and the proposed associated deep Level defect(s) causing the emission. The conduction and valence bands are abbreviated in the usual way as C.B. and V.B., respectively.

Emission (nm)	**Proposed deep level transition**
Violet	Zn_i to V.B. [12]
Blue	Zni to V_{Zn} or C.B. to V_{Zn} [12]
Green	C.B. to V_O, or to V_{Zn}, or C.B. to both V_O and V_{Zn}
Yellow	C.B. to Li, or C.B. to Oi [18]
Orange	C.B. to O_i or Zni to O_i [12]
Red	Lattice disorder along the c-axis(due to Zni)

It has been shown experimentally that the dominant defect in electron-irradiated n-ZnO samples is V_{Zn}, with the Fermi level located 0.2 eV below the conduction band minima [33][39][40]. Neutral V_O was also detected in these experiments. These results imply that charged V_O, if present, will only be in low concentrations below the detection limit due to their high formation energy as discussed above. Nevertheless, other experimental measurements have shown that native defects, and especially V_O deep level defects, can contribute to the unintentional n-type conductivity of ZnO when present as complexes, but not as isolated native point defects [41].

Zinc vacancies are situated 0.9 eV above the valence band minima, and hence a transition from the conduction band (or from a shallow donor) would yield a luminescence around 2.4 eV. This corresponds to the green luminescence observed in ZnO samples grown by many techniques, appearing at 2.4–2.5 eV. Hence, V_{Zn} is widely accepted to contribute to the broad band emission at this green wavelength, although V_O was also suggested as early as 1954 [42] to be the source of this green emission. The result is a deep acceptor transition with states situated 0.72 eV and 1.59 eV above the valence band minima. The other form of Oi is an electrically inactive configuration, which has quite high formation energies for both forms of Oi, except under extremely O-rich environments. This implies that Oi is not expected to be present in high concentrations under equilibrium conditions. The remaining native defects are anti-sites. Zinc anti-sites or oxygen anti-sites consist of zinc or oxygen atoms sitting at the wrong lattice position. All calculations have agreed that ZnO forms shallow donors [43][44].

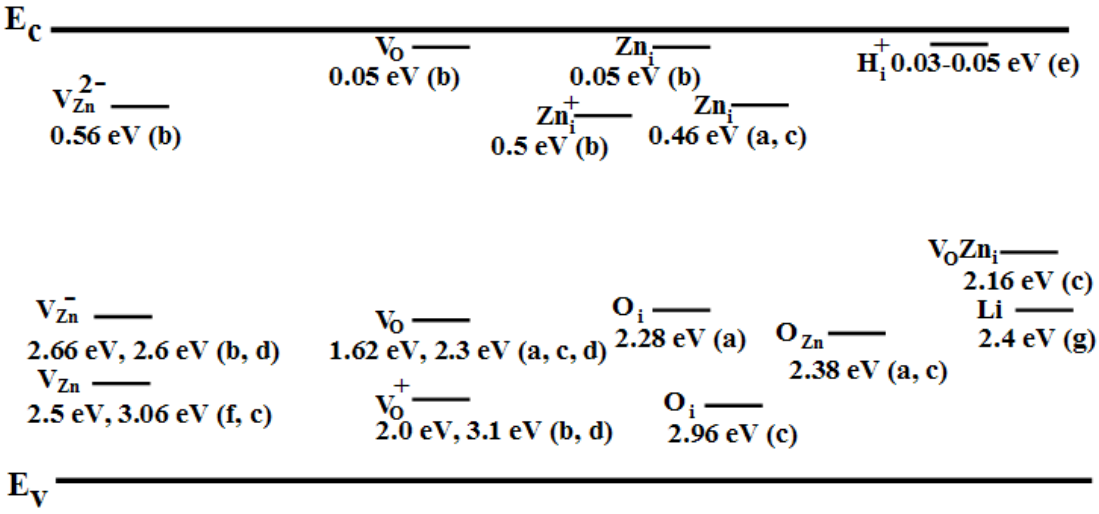

Fig.1.11 Energy levels of the different deep level defects in ZnO reported in the literature by different groups: (a) [45] (b) [46] (c) [47] (d) [48] (e) [49] (f) [33] and (g) [18][50].

Recent calculations indicated that O_{Zn} is a deep acceptor level with two possible transitions situated 1.52 eV and 1.77 eV above the valence band minima. All of the native defects discussed above can exist in different charged states or in a neutral state, and the formation of complexes between native defects and other extrinsic species in ZnO has also been reported. As mentioned above, most of these native defects introduce deep levels at different positions in the band gap, and hence a rather large number of luminescence lines with different energies can be observed. This explains why all of the visible colors have been experimentally observed in different ZnO samples.

1.7Comparison of different semiconducting Materials

ZnO was one of the first semiconductors to be prepared in rather pure form after silicon and germanium. It was extensively characterized as early as the 1950's and 1960's due to its promising piezoelectric/acoustoelectric properties. Wide band gap semiconductors have gained much attention during last decade because of their possible uses as optoelectronic devices in the short wavelength and ultraviolet (UV) portion of the electromagnetic spectrum. These semiconductors such as ZnSe, ZnS, GaN, and ZnO, have shown similar properties with their crystal structures and band gaps. As shown in Table 1.3**,** some of the important properties of these wide band gap semiconductors are summarized.

Table1.3 Comparison of different semiconducting materials

Wide bandgap SC	**Crystal structure**	**Lattice parameter(A^0)**		**Eg (eV at RT)**	**Melting temperature**	**Dielectric constant**		**Excitonic binding energy(MeV)**
		A	**b**			**ε_0**	**ε_∞**	
ZnO	Wurtzite	3.250	5.206	3.37	2248	8.75	3.72	60
GaN	Wurtizite	31.89	51.85	3.4	1973	9.5	5.15	21
ZnSe	Wurtzite	5.667	-	2.7	1790	7.1	5.3	20
ZnS	Zinc blend	3.824	6.261	3.7	2103	9.6	5.7	36

Initially, ZnSe based devices and the GaN based technologies obtained large improvements such as blue and UV light emitting diode and injection laser. ZnSe has produced some defect levels under high current drive. No doubt, GaN are considered to be the best candidate for the optoelectronic devices. However, ZnO has great advantages for light emitting diodes (LEDs) and laser diodes (LDs) over the currently used semiconductors. Recently, it has been introduced that ZnO as II–VI semiconductor is promising for various technological applications, especially for optoelectronic short wavelength light emitting devices due to its wide and direct band gap.

The most important advantage is the high exciton binding energy (60 meV) giving rise to efficient exitonic emission at room temperature. Since ZnO and GaN have almost identical lattice parameters and the same hexagonal wurtzite structure, ZnO can satisfactorily be used as lattice matched substrate in GaN based devices or vice versa. ZnO has excellent radiation hardness among all other semiconductors. This property supplies the uses of ZnO based devices in space applications and high energy radiation environments. Band gap energy can be varied from 3.3 eV up to 4.5 eV with alloying process. Hence it can be used as an active layer in the doubly confined hetero-structured LEDs and quantum well lasers. These unique nanostructures unambiguously demonstrate that ZnO is probably the richest family of nanostructures among all materials, both in structure and properties.

1.8 Literature review

Zinc oxide has excellent properties useful in the development of new optoelectronic devices. Therefore, its physical properties have been exhaustively investigated focusing mainly in the characterization of electrical and optical properties which have rapidly emerged as a promising optoelectronic material suitable to be used in numerous potential technological application, whose examples include thin film gas sensors varistors, ultraviolet and visible lasers, field emitters and solar cell components [51-55].Many dopant employed to enhance the property of ZnO. Mg found most important material to enhance the optical properties.

ZnO crystallizes, a wurtzite hexagonal structure with lattice parameter a=3.24A^0,c=5.20A^0 while MgO posses a cubic phase with a=4.24A^0[56].Although this lattice mismatch but the comparable ionic radii Zn^{+2}=0.60A^0 and Mg^{+2}=0.57A^0,same as a possibility of solid solution formation within the solubility limit and Ohtomo et al.[57]demonstrated 33% of Mg solubility in ZnO by PLD[58][59][60] shows cubic Zn: MgO film with solubility varing form 50% to 86% Baranov et al. [61] reported solid solution of MgxZn1-x($0.32<x<0.67$) at high

temperature and high pressure condition. Moreover, Manoharna et al. [62] used microwave assisted combustion route to achieve a substantial degree of Mg doping > 15-25% in bulk ZnO which is evident from blue shifted optical edge band and a shift emission towards lower wavelength.

ZnO is a well-known greenish white light emitting phosphor for low-voltage vacuum display devices with a relatively high luminescent efficiency Shionoya et al. [63]. Moreover, ZnO due to its bio-compatible character would be a suitable phosphor material (by doping) in biological labeling applications. Many researchers have investigated the emitting properties of ZnO films, including ultraviolet and green emission. Green luminescence of ZnO is a characteristic of phosphors fired in air or under reduced conditions (H_2, ZnS, CO, etc). Lin et al. [64] reported a green luminescent centre in undoped zinc oxide films deposited on silicon substrates by dc reactive sputtering. The intensity of the green peak depends markedly on annealing conditions, but that of the UV peak with annealing conditions varies little. Liu et al. [65] investigated the green and yellow luminescence centers in ZnO and Mn doped ZnO. It was seen that water vapour enhances the green luminescence of ZnO in the surface and causes a two band luminescence phenomenon (green and yellow in the bulk). PL spectra of the ZnO films deposited by Fang et al. [66] showed the blue emission peaks centered at 430 nm. Mordkovich et al. [67] report the discovery and optimization of ZnO-based phosphors using a combinatorial method.

ZnO nanocrystal doped with Cd, Mn, Mg and Fe ions were obtained by Wang et al.[68] the band gap of the nanocrystals can be tuned in the range of 2.9-3.8eV by the use of dopant and most cases, the nanocrystlas are sufficiently to exhibits defect-free band edge luminescence.

Moreover, ZnO doped with Cd and Mg repeated by Li et al.[69]and Lorenz et al.[70]. increase for 7 mol% Mg doped ZnO [74].

ZnO nanocrystal pure and Mn-doped ZnO samples with different percentage of Mn content (1, 2 and 3mol%) were synthesized by a simple solvo-thermal method. Mn doping increases the optical band gap Senthil et al. [75]. These finding shows that nano crystalline samples are displaying blue emission Sagar et al. [76]. In the same way Optical properties of ZnMnO layers grown at low temperature by Atomic Layer Deposition and Metal organic Vapor Phase Epitaxy was used which gives strong absorption, with onset at about 2.1 eV by Godlewski et al. [77]

1.9 Proposed Work

Functional metal oxides have been found to exhibit interesting properties like optical electronic, semiconducting, piezoelectricity etc. Among these metal oxides family, particularly Zinc oxide has become a material of interest among scientific community, due to the commercial importance as additive in paints and protective coating of metals. By keeping all theses functioning properties the present work will an attempt of tailor ZnO structure with Mg and Mn to produce thoroughly efficient phosphor material for luminescent application. These material will be prepared by long structural solid state reaction and chemical rout to achieve doping up to higher percentage and to achieve ZnO Phase and doped Phase at lower temp.

Objectives:

- Synthesis pure Mg doped ZnO via solid state reaction method.
- Preparation of Mg and Mn doped ZnO by chemical route.
- Structural, Morphology, chemical and optical characterization of Mg and Mn doped ZnO systems.

Chapter 2
Methodology and Characterization Techniques

2.1. Materials Selection

The materials used in this study were:

Table 1.4 Materials used in the sample preparation

Name	**Formula**	**Molecular weight g/mol**	**Manufacturing company**
Zinc acetate	$(C_2H_3O_2)\ _2Zn.2H_2O$	219.5	S-D fine chemical Ltd.
Zinc nitrate	$Zn(NO_3)_2.6H_2O$	297.47	Merck
Ethanol	C_2H_5OH	46.06	Merck
Methanol	CH_3OH	32.04186	Merck
Sodium hydroxide	NaOH	40.0	S-D fine chemical Ltd.
Magnesium chloride dehydrate	$MgCl_2.6H_2O$	203.30	Merck
Manganese chloride tetra hydrate	$MnCl_2.4(H_2O)$	197.90	Merck
Ammonia solution	NH_3	17.03	Merck
Zinc Oxide	ZnO	81.37	Merck
Magnesium Oxide	MgO	40.30	S-D fine chemical Ltd.

2.2Synthesis of doped Zinc Oxide

2.2.1Synthesis of Mg doped ZnO via solid state reaction

Doped ZnO were prepared by solid state reaction. In this work plan, we used commercially available ZnO (Merck) and MgO (S.D.Fine) in different proportion and kept into in furnace at 900^{O}C for 2 hours.

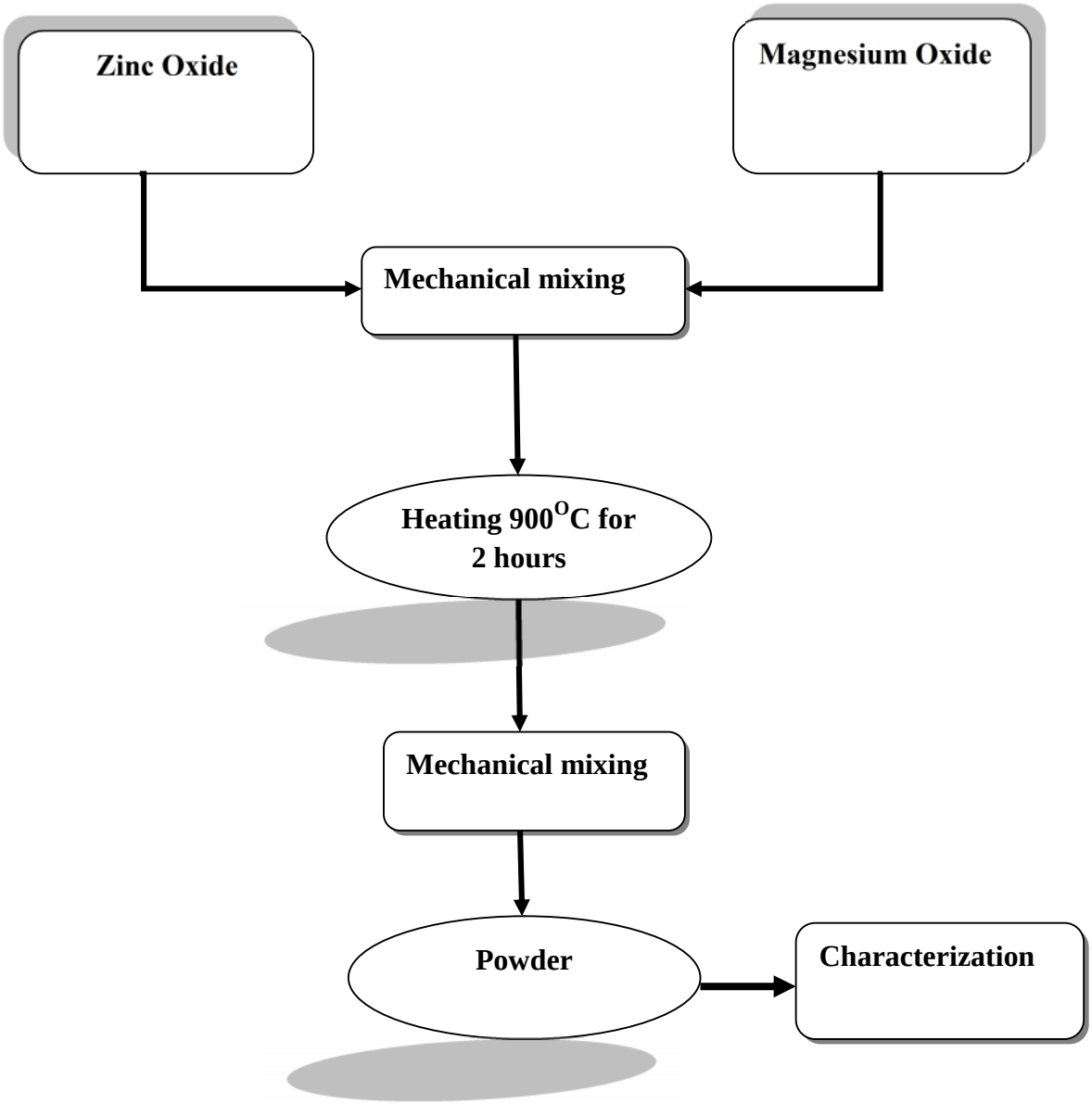

Fig 2.1 Flow chart of Mg doped ZnO synthesized by solid state reaction

Table 1.5 Materials taken for the synthesis of Mg doped ZnO by solid state reaction

Sample Name	Weight of ZnO/g	Weight of MgO/g	Doping % Mg
ZnO:Mg 1%	10	0.1	1
ZnO:Mg 3%	10	0.3	3
ZnO:Mg 5%	10	0.5	5
ZnO:Mg 9%	10	0.9	9
ZnO:Mg 11%	10	1.1	11
ZnO:Mg 15%	10	1.5	15

2.2.2 Synthesis of Mg doped ZnO by co-precipitation method

2.2.2.1 Synthesis of Mg doped ZnO by co-precipitation method in distilled water

In the typical procedure the precursor materials of matrix and the dopant were taken in the three neck glass flask in appropriate amount. The reaction mixture was stirred for 1 hour at room temperature. The two contents were mixed and followed by the addition of ammonium solution. The formed gel was washed with distilled water .The remaining gel was further stirred at 80^0C for 6h.The product was filtered out and dried at 90^0C for 2 hours. Finally, the obtained powder was characterized by using number of technique.

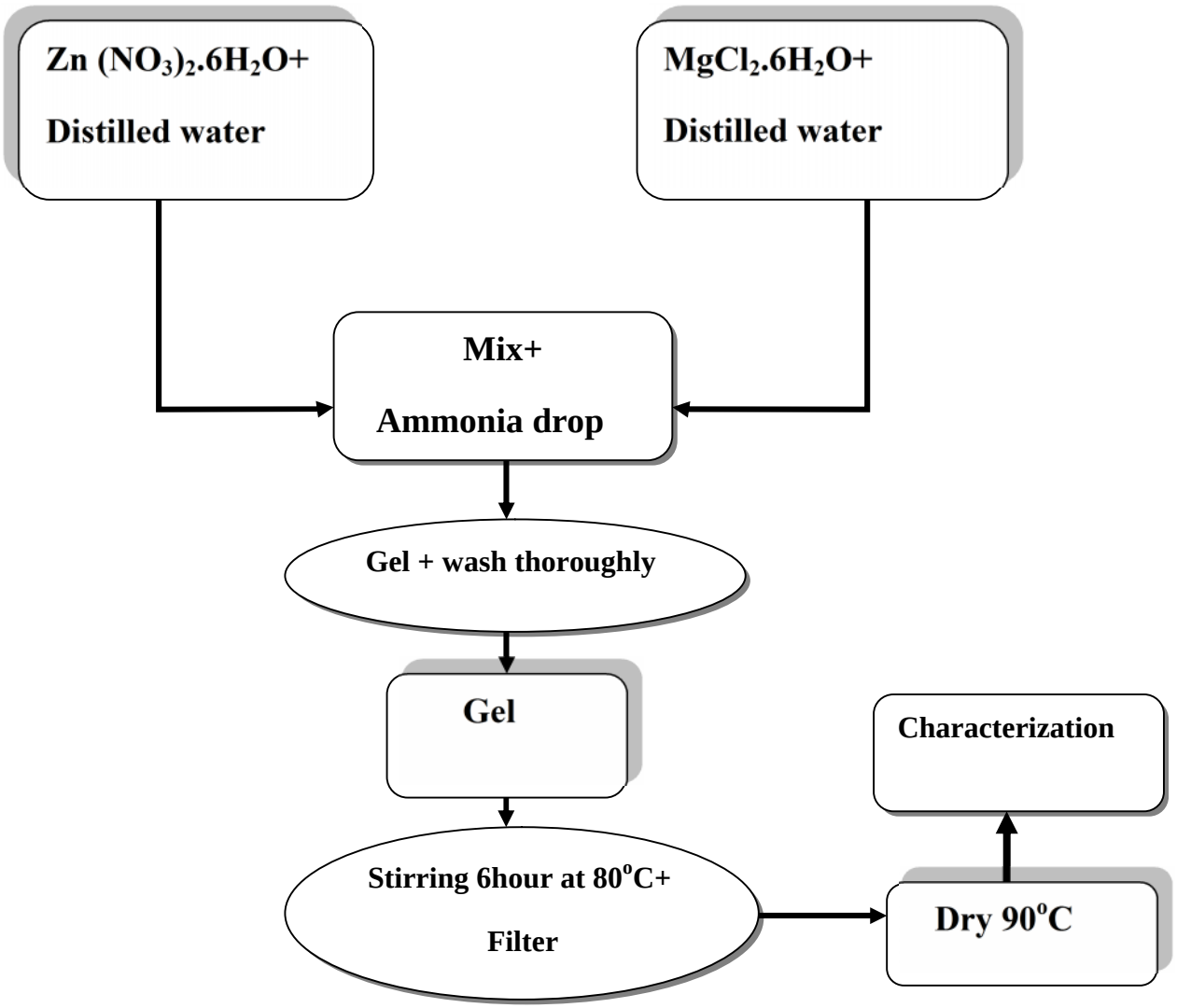

Fig2.2 Flow chart of Mg doped ZnO by co-precipitation method in distilled water

Table 1.6 Materials taken for the synthesis of Mg doped ZnO by co-precipitation method in distilled water

Sample Name	Zinc Nitrate/g	Distilled water/ml	Magnesium chloride/g	Distilled water/ml	Doping % of Mg
ZnO:Mg 1%	11.9	180	0.27	5	1
ZnO:Mg 3%	11.9	180	0.81	5	3
ZnO:Mg 5%	11.9	180	1.35	5	5
ZnO:Mg 9%	11.9	180	2.43	5	9
ZnO:Mg 11%	11.9	180	2.97	5	11
ZnO:Mg 15%	11.9	180	4.05	5	15

2.2.2.2 Synthesis of Mg doped ZnO via co-precipitation method in ethanol

Zinc acetate [$(C_2H_3O_2)_2Zn.2H_2O$] and C_2H_5OH were used as a precursor material and the solvent, respectively .The precursor material and dopant[$MgCl_2.6H_2O$] were mixed in three neck flask .The mixed materials were refluxed at 70^0C for 2 hour. The appropriate amounts of NaOH were added to the reaction media to adjust the PH in basic medium. The final product was filtered out via vigorous washing with ethanol. The obtained powder dried at 90^0C for 2 hours [28].

Fig 2.3 Experimental setup for co-precipitation method

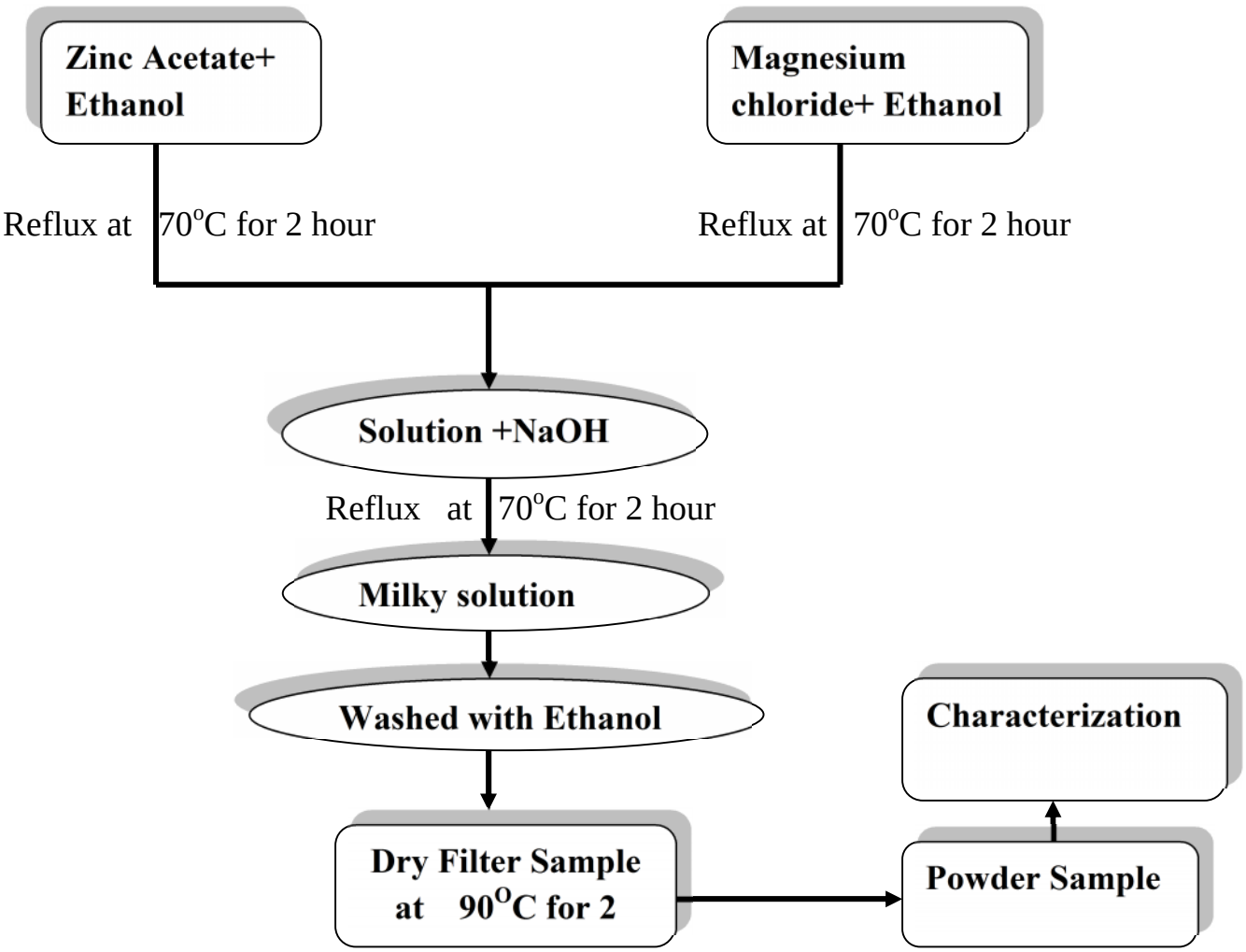

Fig 2.4 Flow chart of Mg doped nano ZnO synthesized by co precipitation method in ethanol

Table 1.7 Materials taken for the Synthesis of Mg doped ZnO by co precipitation method in ethanol

Sample Name	Zinc acetate/g	Magnesium Chloride/g	Ethanol/ml	NaoH/g	Doping Mg wt%
ZnO	2.19	--------	200	1.60	-----
ZnO:Mg 1%	2.19	0.02032	200	1.60	1
ZnO:Mg 3%	2.19	0.0609	200	1.60	3
ZnO:Mg 5%	2.19	0.1016	200	1.60	5
ZnO:Mg 7%	2.19	0.1422	200	1.60	7
ZnO:Mg 9%	2.19	0.1828	200	1.60	9
ZnO:Mg 11%	2.19	0.2235	200	1.60	11
ZnO:Mg 15%	2.19	0.3048	200	1.60	15

2.2.2.3 Synthesis of Mg doped ZnO via co-precipitation method in methanol

The procedure was same as discussed for ethanol.

Table 1.8 Materials taken for the synthesis of Mg doped ZnO by co precipitation method in methanol

Sample Name	Zinc acetate/g	Magnesium Chloride/g	methanol/ml	NaoH/g	Doping Mg wt%
ZnO	2.19	--------	200	1.60	-----
ZnO:Mg 1%	2.19	0.02032	200	1.60	1
ZnO:Mg 3%	2.19	0.0609	200	1.60	3
ZnO:Mg 5%	2.19	0.1016	200	1.60	5
ZnO:Mg 7%	2.19	0.1422	200	1.60	7
ZnO:Mg 9%	2.19	0.1828	200	1.60	9

2.2.3 Synthesis of Mn doped ZnO via co-precipitation method in methanol

Same procedure was employed for the synthesis of Mn doped ZnO as discussed above in the case of Mg doped ZnO.

Table 1.9 Materials taken for the Synthesis of Mn doped ZnO by co precipitation method in methanol

Sample Name	Zinc acetate/g	Manganese Chloride/g	Methanol/ml	NaoH/g	Doping Mg wt%
ZnO	2.19	--	200	1.60	--
ZnO:Mn 1%	2.19	0.0197	200	1.60	1
ZnO:Mn 5%	2.19	0.0985	200	1.60	5
ZnO:Mn 7%	2.19	0.1379	200	1.60	7
ZnO:Mn 9%	2.19	0.1778	200	1.60	9

2.2.4 Synthesis of Zn doped MgO via solid state reaction

Same procedure was employed to prepare these samples as shown in flow chart 2.1.

Table 2.0 Materials taken for the Synthesis of Zn doped MgO by solid state reaction

Sample Name	**Weight of MgO/g**	**Weight of ZnO/g**	**Doping %Zn**
MgO:Zn 1%	10	0.1	1
MgO:Zn 3%	10	0.3	3
MgO:Zn 5%	10	0.5	5
MgO:Zn 9%	10	0.9	9
MgO:Zn 11%	10	1.1	11
MgO:Zn 15%	10	1.5	15

2.3 Characterization techniques

2.3.1XRD

X-ray diffraction is a versatile, non-destructive analytical method for identification and quantitative determination of various crystalline forms, known as 'phases' of compound present in powder and solid samples. Diffraction occurs as waves interact with a regular structure whose repeat distance is about the same as the wavelength. The phenomenon is common in the natural world, and occurs across a broad range of scales. For example, light can be diffracted by a grating having scribed lines spaced on the order of a few thousand angstroms, about the wavelength of light. It happens that X-rays have wavelengths on the order of a few angstroms, the same as typical inter-atomic distances in crystalline solids. That means X-rays can be diffracted from minerals which, by definition, are crystalline and have regularly repeating atomic structures. When certain geometric requirements are met, X-rays scattered from a crystalline solid can constructively interfere, producing a diffracted beam. In 1912, W. L. Bragg recognized a predictable relationship among several factors.

1. The distance between similar atomic planes in a mineral (the interatomic spacing) which we call the d-spacing and measure in angstroms.
2. The angle of diffraction which we call the theta angle and measure in degrees. For practical reasons the diffract meter measures an angle twice that of the theta angle. Not surprisingly, we call the measured angle '2-theta'.
3. The wavelength of the incident X-radiation, symbolized by the Greek letter lambda and, in our case, equal to 1.54 angstroms.

2.3.1.1Bragg's Law

Since atoms are arranged periodically in a lattice, x-rays scattered from a crystalline solid can constructively interfere, producing a diffracted beam through these atoms. In 1912, W. L.
Bragg recognized a predictable relationship among several factors. These factors are combined in Bragg's law

$$n \lambda = 2d \sin\Theta \qquad \text{……..(2)}$$

n = an interger-1, 2, 3….etc (n=1 for our calculations)

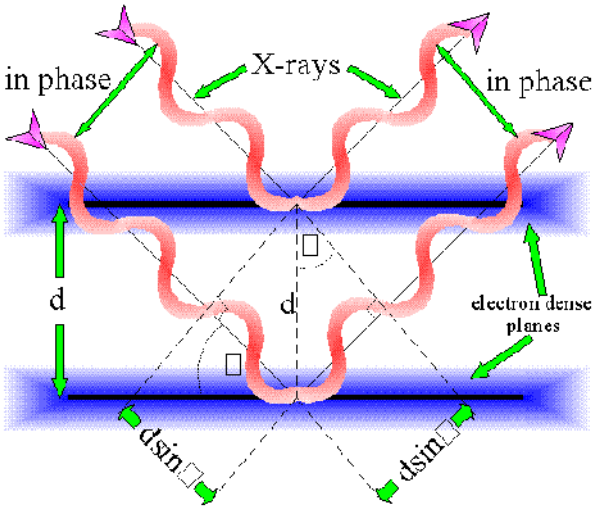

Fig2.6 Bragg reflection

2.3.1.2Crystallite size measurement: Debye Scherer's Formula

Phase identification using x-ray diffraction depends on the positions of the peaks in a diffraction profile as well as the relative intensities of these peaks to some extent. Another aspect of the diffraction from material is the importance to consider how diffraction peaks are changed by the presence of various types of defects such as small number of dislocations in crystals with dimensions of millimeters. Small size of grain size can be considered as another kind of defect and can change diffraction peak widths. Very small crystals cause peak boarding. The crystallite size is easily calculated as a function of peak width (specified as the full-width at half maximum peak intensity (FWHM), peak position and wavelength. The Debye Scherrer's formula [80].

$$D=0.9\ \lambda/\beta\ \cos\theta \qquad \ldots\ldots\ldots\ldots\ldots\ldots\ (3)$$

Where D is average particle size, λ is wavelength; β is full width half maximum

2.3.2Scanning Electron Microscopy (SEM):

The scanning electron microscope (SEM) is a type of electron microscope that images the sample surface by scanning it with a high-energy beam of electrons in a raster scan pattern. The electrons interact with the atoms that make up the sample producing signals that contain information about the sample's surface topography, composition and other properties such as electrical conductivity.

The types of signals produced by an SEM include secondary electrons, back-scattered electrons (BSE), characteristic X-rays, light (cathodoluminescence), specimen current and transmitted electrons. Secondary electron detectors are common in all SEMs, but it is rare that a single machine would have detectors for all possible signals. The signals result from interactions of the electron beam with atoms at or near the surface of the sample. In the most common or standard detection mode, secondary electron imaging or SEI, the SEM can produce very high-resolution images of a sample surface, revealing details about less than 1 to 5 nm in size

Scanning electron microscopy (SEM) is basically a type of electron microscope. SEM is used for various purposes;

- Topographic studies.
- Microstructure analysis.
- Elemental analysis if equipped with appropriate detector (energy/wavelength dispersive x-rays).
- Chemical composition.
- Elemental mapping

Fig.2.7 Experimental set up of SEM

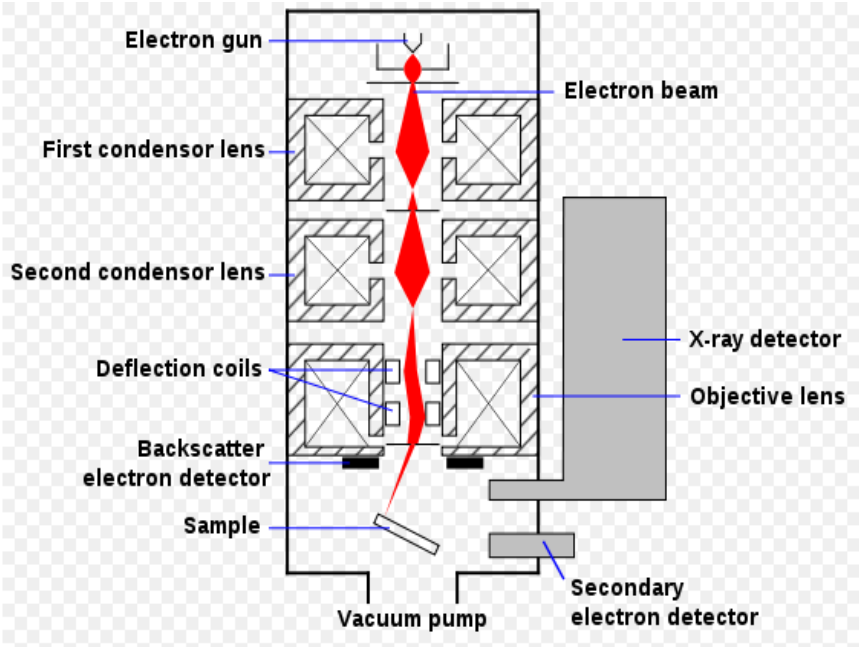

Fig 2.8 Schematic illustration of the SEM

In SEM, Primary electrons are thermonically or field emitted by a cathode filament (W or Lab) or a field emission gun (W-tip) and after that accelerated with high energy typically 1-30KeV. The electron beam is steered with scanning coils over the area of the interest. Upon interaction with material, the primary electrons decelerate as well as losing his energy, transfer it in elastically to other atomic electron and to the lattice. Due to continuous scattering events the primary beam spread up with different energies depending on source origin.

Secondary electrons (1-50eV) are mostly used for the imaging the topographically contrast and reproduce the surface. High energy elastically backscattered electrons depends on the atomic number (Z) of the element, which is useful to obtain Z-constrat. X-ray characteristic can be used to qualitatively and quantitatively analyze the elemental composition and distribution in the sample.

2.3.2.1 Illustration of SEM setup

The experimental setup consists of an electron gun, column, scanning system, substrate chamber, detectors.

Electron gun

It is based on the thermal emission. The electron source is commonly a tungsten (W) or lanthanum hex boride (LaB6) tip. Electrons are emitted during heating.

Column

The column consists of two electromagnetic lenses acting on the electron beam. The first lens, the condenser lens produces most of the beam demagnification, while the second, objective lens focuses the beam onto the sample. In column, a beam shaper called stigmator, the stigmator can create a magnetic field around the beam to restore it in a circular cross section.

Scanning system

To get image on the display the beam should be scanned over the specimen and the display tube. Information from any point on the sample can then reproduced in the same relative position on the display.

Substrate chamber

The substrate holder depends on the different size and shape of the sample. The sample can be moved in three dimensions, as well as rotated and titled.

Detector

The most detector types used for secondary electrons are the scintillation detector. It can be used for primary electrons.

X-ray detector

Spectrometers for detection and analysis of X-ray s are based on either of two principles.

- Wavelength dispersive X-ray (WDX); determines the wavelength of the X-rays.
- Energy dispersive X-ray (EDX); determine the energy of the X-rays.

2.3.3FTIR Spectra

Fourier transform infrared (FTIR) spectroscopy is a measurement technique that allows one to record infrared spectra. Infrared light is guided through an interferometer and then through the sample . A moving mirror inside the apparatus alters the distribution of infrared light that passes through the interferometer. The signal directly recorded, called an "interferogram", represents light output as a function of mirror position. A data-processing technique called Fourier transform turns this raw data into the desired result (the sample's spectrum): Light output as a function of infrared wavelength (or equivalently, wavenumber). As described above, the sample's spectrum is always compared to a reference.

.

Fig 2.9: Fourier transforms infrared (FTIR) spectrometry

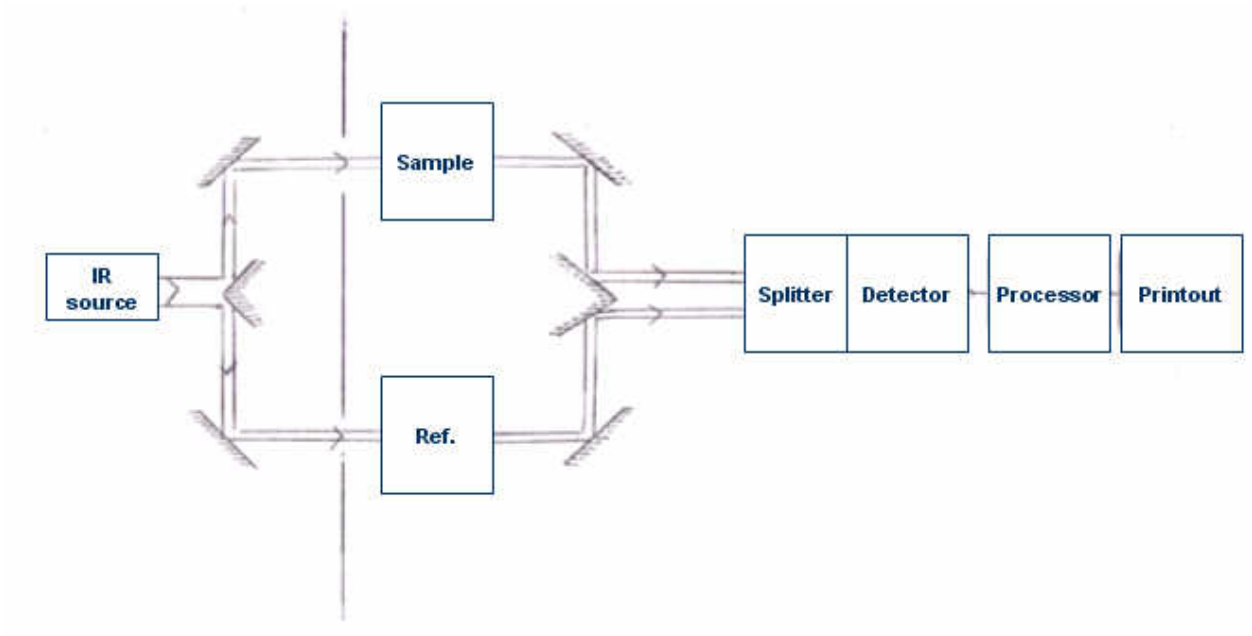

Fig2.10 Schematic illustration of the FTIR

The experimental set up shown is in figure 2.9. In infrared spectroscopy, IR radiation is passed through a sample. Some of the infrared radiation is absorbed by the sample and some of it is passed through (transmitted). The resulting spectrum represents the molecular absorption and transmission, gives information of type of bonding in the sample. This makes infrared spectroscopy useful for several types of analysis

- FTIR can identify unknown materials
- FTIR can determine the quality or consistency of a sample
- FTIR can determine the amount of components in a mixture

The original infrared instruments were of the dispersive type. These instruments separated the individual frequencies of energy emitted from the infrared source. This was accomplished by the use of a prism or grating. A grating is a more modern dispersive element which better separates the frequencies of infrared energy. The detector measures the amount of energy at each frequency which has passed through the sample. This results in a spectrum which is a plot of intensity vs. frequency.

Fourier Transform Infrared (FT-IR) spectrometry was developed in order to overcome the limitations encountered with dispersive instruments. The main difficulty was the slow scanning process. A method for measuring all of the infrared frequencies simultaneously, rather than

individually, was needed. A solution was developed which employed a very simple optical device called an interferometer. The interferometer produces a unique type of signal which has all of the infrared frequencies "encoded" into it. The signal can be measured very quickly, usually on the order of one second. Thus the time element per sample is reduced to a matter of a few seconds rather than several minutes.

2.3.4Ultra-Voilet spectroscopy

Ultraviolet-visible spectroscopy refers to absorption spectroscopy in the ultraviolet-visible spectral region. This means it uses light in the visible and adjacent (near-UV and near-infrared (NIR)) ranges. The absorption in the visible range directly affects the perceived color of the chemicals involved. In this region of the electromagnetic spectrum, molecules undergo electronic transitions. This technique is complementary to fluorescence spectroscopy, in that fluorescence deals with transitions from the excited state to the ground state, while absorption measures transitions from the ground state to the excited state.

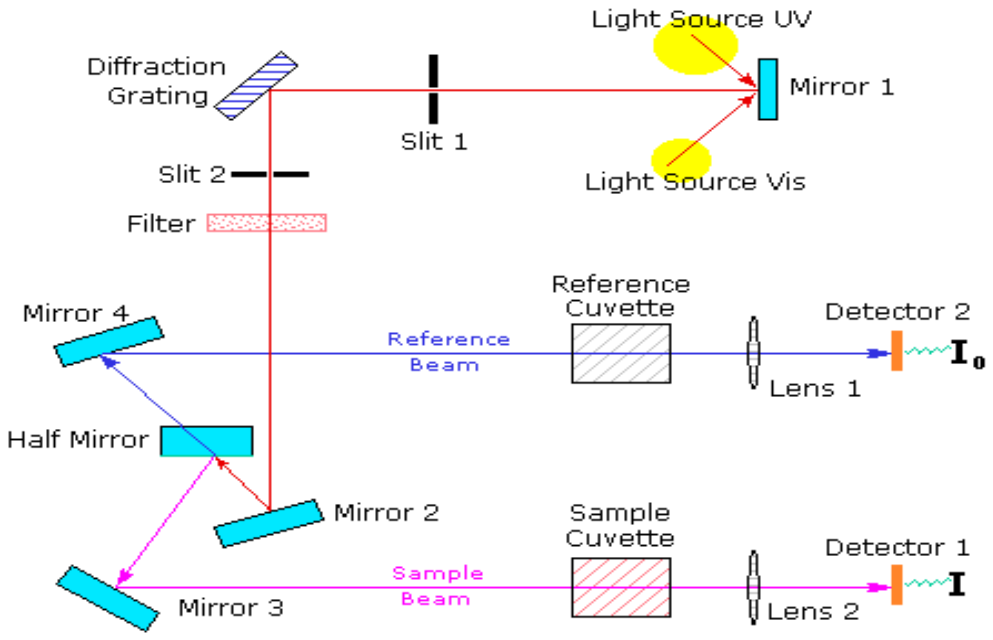

Fig 2.11 Schematic diagram of UV spectroscopy

A diagram (Fig.2.11) of the components of a typical spectrometer is shown in the following diagram. The functioning of this instrument is relatively straightforward. A beam of light from a

visible and/or UV light source (colored red) is separated into its component wavelengths by a prism or diffraction grating.

Each monochromatic (single wavelength) beam in turn is split into two equal intensity beams by a half-mirrored device. One beam, the sample beam (colored magenta), passes through a small transparent container (cuvette) containing a solution of the compound being studied in a transparent solvent. The other beam, the reference (colored blue), passes through an identical cuvette containing only the solvent. The intensities of these light beams are then measured by electronic detectors and compared. The intensity of the reference beam, which should have suffered little or no light absorption, is defined as I_0. The intensity of the sample beam is defined as I. Over a short period of time, the spectrometer automatically scans all the component wavelengths in the manner described. The ultraviolet (UV) region scanned is normally from 200 to 400 nm, and the visible portion is from 400 to 800 nm.

If the sample compound does not absorb light of of a given wavelength, $I = I_0$. However, if the sample compound absorbs light then I is less than I_0, and this difference may be plotted on a graph versus wavelength.. Absorption may be presented as transmittance ($T = I/I_0$) or absorbance ($A = \log I_0/I$).

Different compounds may have very different absorption maxima and absorbance. Intensely absorbing compounds must be examined in dilute solution, so that significant light energy is received by the detector, and this requires the use of completely transparent (non-absorbing) solvents. The most commonly used solvents are water, ethanol, hexane and cyclohexane. Solvents having double or triple bonds, or heavy atoms (e.g. S, Br & I) are generally avoided. Because the absorbance of a sample will be proportional to its molar concentration in the sample cuvette, a corrected absorption value known as the molar absorptivity is used when comparing the spectra of different compounds. This is defined as:

Molar Absorptivity, $\varepsilon = A/ c\, l$ (where *A*= absorbance, **c** = sample concentration in moles/liter & **l** = length of light path through the cuvette in cm.)

2.3.5Photoluminescence Spectra

Photoluminescence (abbreviated as PL) is a process in which a substance absorbs photons (electromagnetic radiation) and then re-radiates photons. Quantum mechanically, this can be described as an excitation to a higher energy state and then a return to a lower energy state accompanied by the emission of a photon. This is one of many forms of luminescence (light emission) and is distinguished by photo excitation (excitation by photons), hence the prefix photo. The period between absorption and emission is typically extremely short, in the order of 10 nanoseconds. Under special circumstances, however, this period can be extended into minutes or hours.All solids, including semiconductors, have “energy gaps” for the conducting electrons. In order to understand the concept of a gap in energy, first consider that some of the electrons in a solid are not firmly attached to the atoms, as they are for single atoms, but can hop from one atom to another. These loosely attached electrons are bound in the solid by differing amounts and thus have much different energy.

Electrons having energies above a certain value are referred to as conduction electrons, while electrons having energies below a certain value are referred to as valence electrons. This is shown in the diagram where they are labeled as conduction and valence bands. The word band is used because the electrons have a multiplicity of energies in either band. Furthermore, there is an energy gap between the conduction and valence electron states. Under normal conditions electrons are forbidden to have energies between the valence and conduction bands.

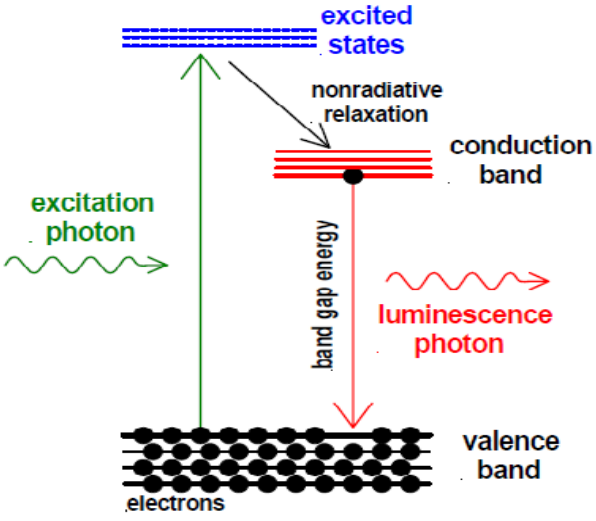

Fig 2.12 Mechanism of Photoluminescence

If a light particle (photon) has energy greater than the band gap energy, then it can be absorbed and thereby raise an electron from the valence band up to the conduction band across the forbidden energy gap. (See diagram.) In this process of photo excitation, the electron generally has excess energy which it loses before coming to rest at the lowest energy in the conduction band. At this point the electron eventually falls back down to the valence band. As it falls down, the energy it loses is converted back into a luminescent photon which is emitted from the material. Thus the energy of the emitted photon is a direct measure of the band gap energy, E_g The process of photon excitation followed by photon emission is called photoluminescence

2.3.5.1Photoluminescence Spectra Setup

The spectrofluorophotometer irradiates a sample with excitation light and measures the photoluminescence spectra emitted from the irradiated sample to perform a qualitative or quantitative analysis. A typical configuration of the spectrofluorophtometer RF-5301PC is schematically described below:

Fig2.13 Photoluminescence Spectroscopy RF-5301PC

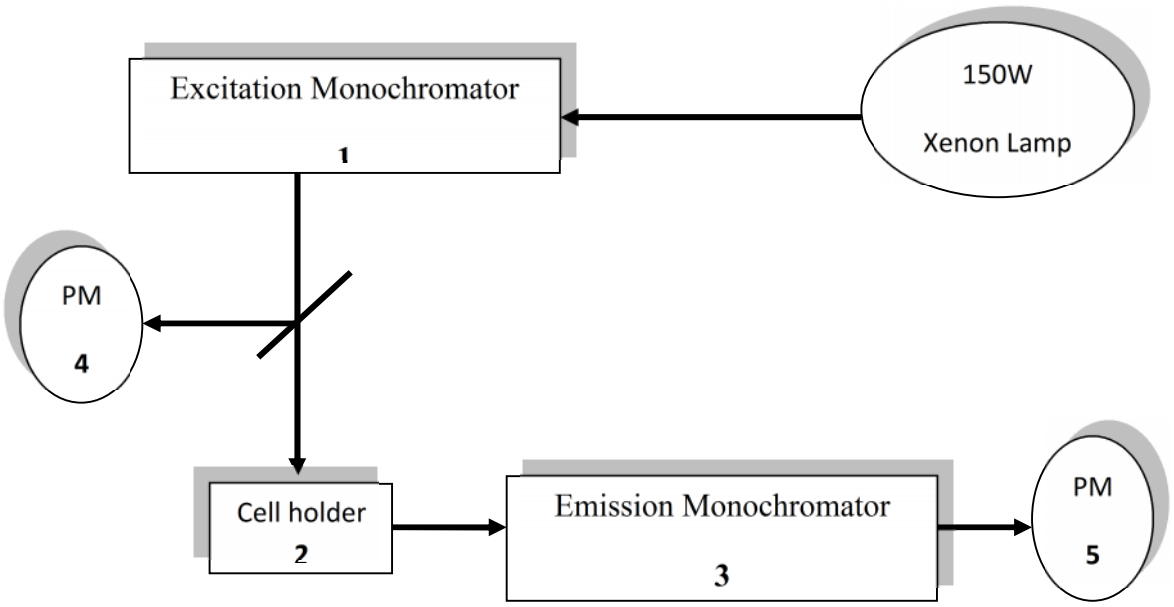

Fig 2.14: Constitution of RF-5301PC

1. The excitation monochrpomator isolated a band of a particular wavelength from the light form Xenon lamp to obtain excitation light. Since brighter excitation light will contribute to higher sensitivity of the spectroflurorophotometer, the exaction monochromatic incorporate a diffraction grating with a larger aperture to collect the largest possible amount of light.

2. The cell holder holds a cell filled with sample.

3.The emission monochromator selectively receives luminescence emitted from the sample and its photomultiplier tube measures the intensity of the fluororescence.This monochromator has a diffraction grating whose size is the same as that of the excitation monochromator to collect the greatest possible amount of light.

4. The photomultiplier tube is for monitoring .Generally, the Xenon lamps used on spectrofluorophotometers are characterized by very high emission intensity and an uninterrupted radiation spectrum. However, their tendency to unstable light emission will result in tarter signal noise if no countermeasure is incorporated .In addition, the non-uniformity in the radiation spectrum of the Xeon lamp and in the spectral sensitivity characteristics of the photomultiplier tube cause distortion in to spectrum. To overcome these factored the phtomutipleire tube monitor a portion of excitation light and feeds the resultant signal back to the photomultiplier tube for fluorescence scanning.

Chapter3
Result and discussion

This chapter summarized the results obtained from XRD, SEM, FTIR, UV, PL to understand the structural morphology, chemical and optical behavior of pure and doped samples derived from solid state reaction method and chemical route. Finally, we conclude our observation.

3.1 XRD Analysis

The XRD pattern obtained for commercially available ZnO and MgO shown in figure 3.1.the well crystalline peak obtained in the ZnO and MgO sample corresponds to the (100),(002),(101),(102),(110),(103) and (002),(220) planes respectively. Which refer to the wurtzite hexagonal structure of ZnO and Halite Octahedral structure of MgO. These samples used as standard systems for the other doped samples.

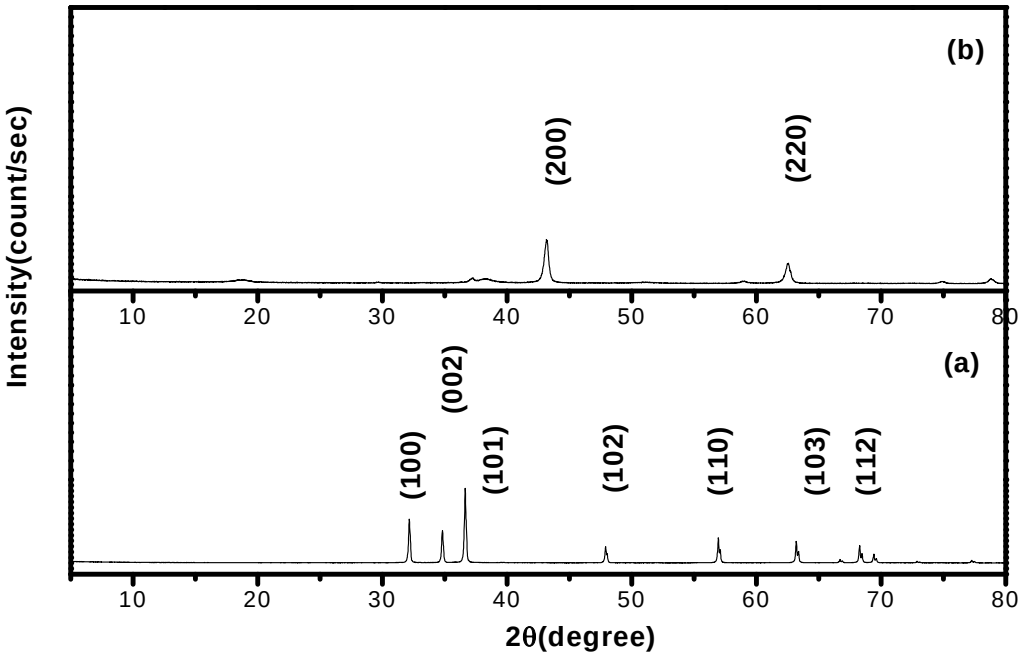

Fig 3.1: XRD pattern for the pure commercially available (a) ZnO (b) MgO

3.1.1 XRD analysis of Mg doped ZnO synthesized by solid state reaction method

The XRD patterns of the Mg doped ZnO synthesized by solid state reaction method are shown in figure3.2. The peak observed at 2θ = 31.50, 33.760, 35.90, 47.230, 56.180, 62.20 and 67.60 refer to the lattice plane (100), (002), (101), (102), (110), (103) and (112) respectively, indicative of wurtzite hexagonal structure of ZnO (matched JCPDS data card No.67849). All the samples were found single phase up to higher concentration of Mg(15%). Although small reflectance observed at 2 theta = 43^0 for 15wt%concentration of dopant may correspond to the MgO. These XRD results revels that Mg fit in the valance site of the Zn ion without disturbing the crystal structure.

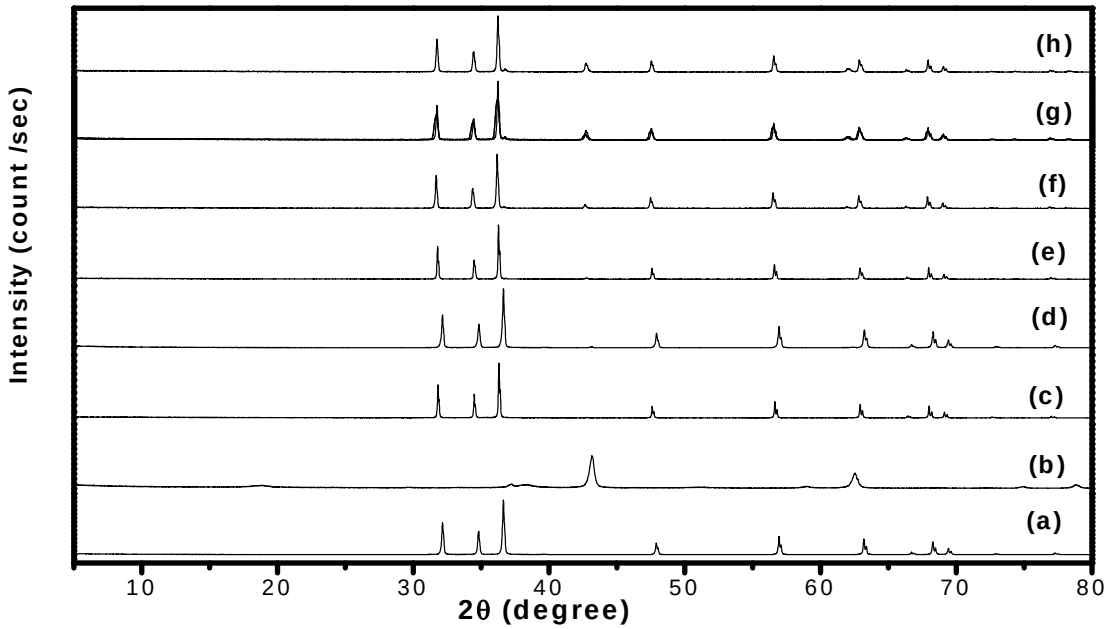

Fig3.2: XRD patterns of Mg doped ZnO synthesized via solid state reaction method **(a)** ZnO_st **(b)** MgO_st **(c)**ZnO:Mg1% **(d)** Mg3% **(e)** Mg5% **(f)** Mg9% **(g)** Mg11% **(h)**Mg15%

3.1.2 XRD analysis of Mg doped ZnO synthesized by Co-precipitation method

3.1.2.1 XRD analysis of Mg doped ZnO synthesized by Co-precipitation method in distilled water

The XRD patterns of the Mg doped ZnO synthesized by co precipitation method are shown in the figure 3.3.The peak observed at 2θ = 31.50, 33.760, 35.90, 47.230, 56.180, 62.20 and 67.60 correspondence to the lattice plane (100), (002), (101), (102), (110), (103) and (112) respectively for all samples, indicative of wurtzite hexagonal structure of ZnO, well matched

with JCPDS card no67849. The XRD results also revealed that no impurity peak obtained up to 7% and Mg ion fit perfectly in Zn valence site without disturbing the crystal structure. As we increase the concentration of Mg, the structure has been disturbed as number of impurity peaks has been found.

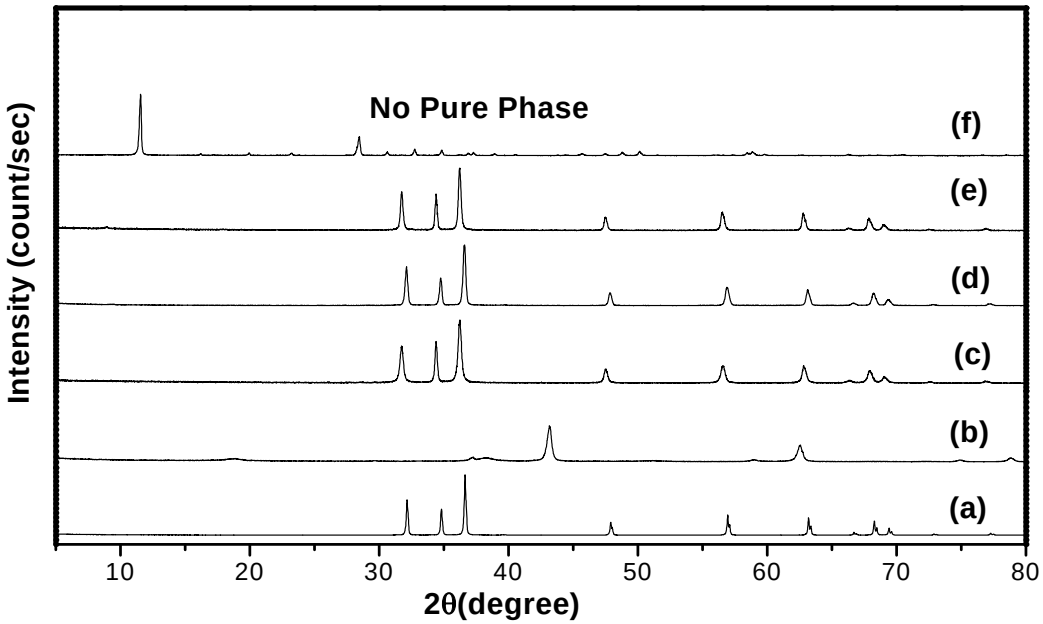

Fig3.3: XRD spectra of Mg doped ZnO synthesized via Co-precipitation method in distilled water **(a)** ZnO_st **(b)** MgO_st **(c)**ZnO:Mg1% **(d)** Mg3% **(e)**Mg7%

3.1.2.2 XRD analysis of Mg doped ZnO synthesized by Co-precipitation method in ethanol

The XRD patterns of the Mg doped ZnO synthesized by co-precipitation method in the presence of ethanol are shown in figure 3.4. The peaks appeared at 2θ = 31.50, 33.760, 35.90, 47.230, 56.180, 62.20 and 67.60 correspondence to the lattice plane (100), (002), (101), (102), (110), (103) and (112) respectively, indicating the formation of wurtzite hexagonal structure of ZnO. It was noticed that ZnO prepared by this method in the dilute medium of ethanol accept the dopant ion up to higher concentration (15%). A small impurity diffraction peaks observed at 2theta=45.69^0 ZnO at higher concentrations not corresponds to the matrix nor to the dopant ion.

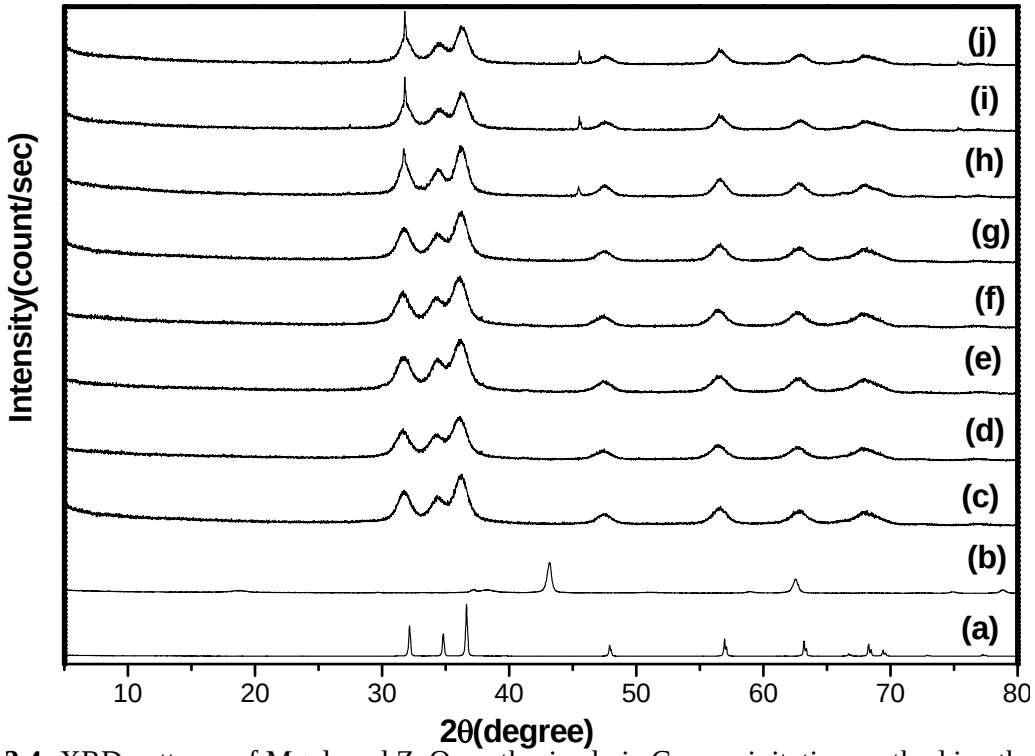

Fig 3.4: XRD patterns of Mg doped ZnO synthesized via Co-precipitation method in ethanol **(a)** ZnO_st **(b)** MgO_st **(c)** ZnO_P**(d)**ZnO:Mg1% **(e)** Mg3% **(f)** Mg5% **(g)** Mg7% **(h)** Mg9% **(i)** Mg11% **(j)** Mg15%

3.1.2.3 XRD analysis of Mg doped ZnO synthesized by Co-precipitation method in methanol

In the similar way Methanol was also employed as solvent media to lower the reaction temperature and analyzes its effect on pure and doped ZnO samples. The corresponding XRD patterns of synthesized are shown in figure3.5. Peaks appeared at 2θ = 31.50, 33.760, 35.90, 47.230, 56.180, 62.20 and 67.60 attributed the to the lattice plane (100), (002), (101), (102), (110), (103) and (112) respectively for all samples, confirming of wurtzite hexagonal structure of ZnO. The average particle size calculated for these synthesized samples is ranging between 300-400nm.

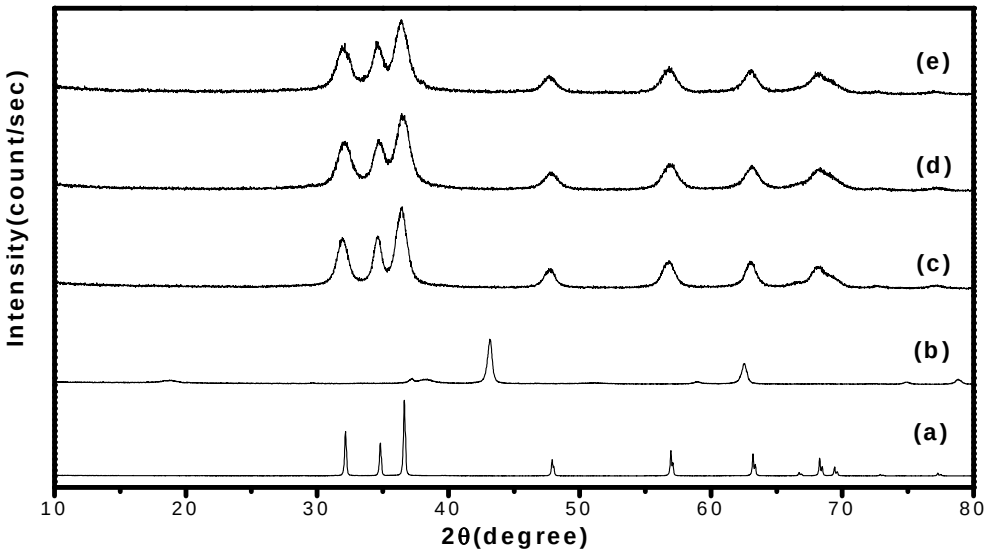

Fig3.5: XRD patterns of Mg doped ZnO **s**ynthesized via Co-precipitation method in methanol **(a)** ZnO_st **(b)** MgO_st **(c)**ZnO: P**(d)** ZnO:Mg3% **(e)**Mg9%

From the above XRD analysis it can be concluded that both solid sate reaction and chemical approach gives the pure phase up to the higher doping concentration of Mg ion on the Zn valance site. However, it was remarkable to note that particle size was found higher in samples prepared by solid state reaction method than chemical route. In distilled water, system shows successfully doping upto7%, though we can dope Mg ion up to15% in ethanol and methanol medium. It is quite reasonable to say that as we decreased in the temperature of the reaction, particle size and doping efficiency enhanced. Chemical route was found better prospective that that of solid state reaction method according to our analysis.

3.1.3 XRD analysis of Mn doped ZnO synthesized by Co-precipitation method in methanol

Figure 3.6 presenting the diffraction patterns of Mn doped ZnO synthesized by co precipitation method in alcoholic medium .Diffraction peaks appeared at 2θ = 31.50, 33.760, 35.90, 47.230, 56.180, 62.20 and 67.60 attributed the to the lattice plane (100), (002), (101), (102), (110), (103) and (112) respectively for all samples, confirming of wurtzite hexagonal structure of ZnO.

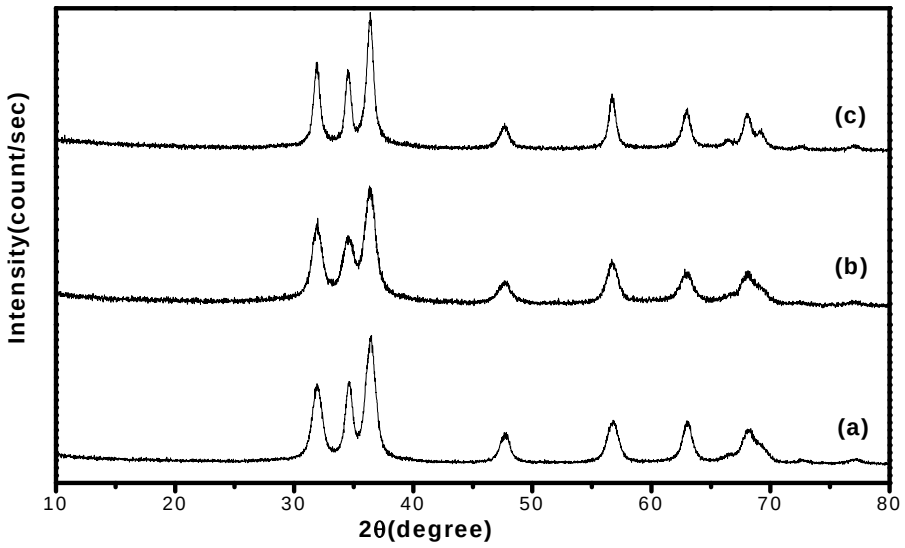

Fig3.6: XRD patterns of Mn doped ZnO synthesized via Co-precipitation method in methanol **(a)** ZnO_P **(b)** ZnO: Mn3% **(c)** Mn9%

3.1.4 XRD analysis of Zn doped MgO synthesized by solid state reaction

Finally we made an attempt to dope Zn on the MgO matrix. The XRD patterns of the Zn

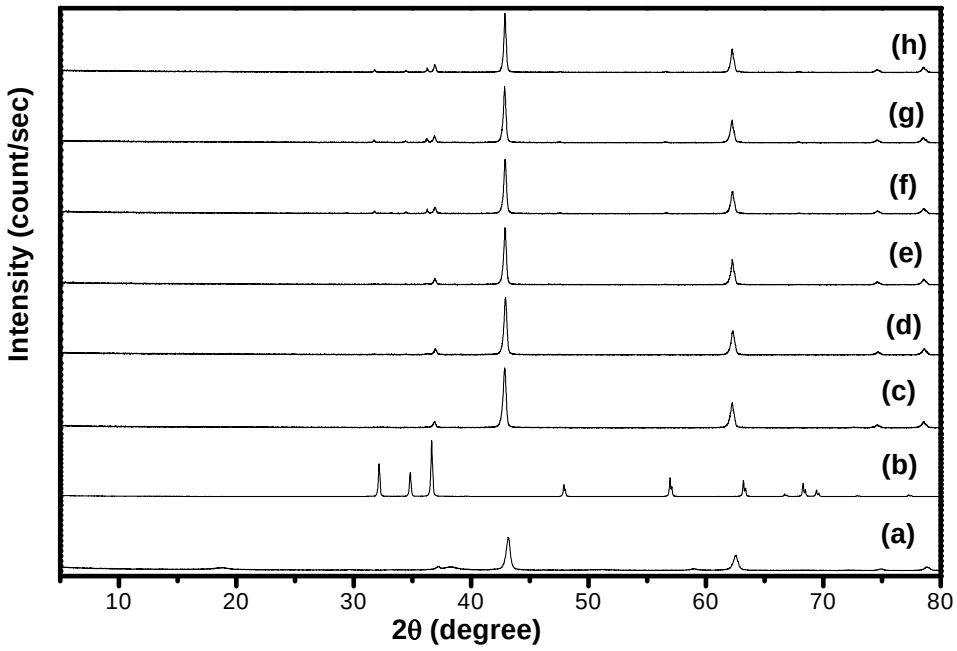

Fig3.7: XRD pattern of Zn doped MgO by solid state reaction **(a)** MgO_st **(b)** ZnO_st **(c)**MgO**:**Zn1% **(d)** Zn3% **(e)**Zn5% **(f)** Zn9% **(g)** Zn11% **(h)** Zn15%

doped MgO synthesized by solid state reaction are shown in figure3.7. The peaks observed at 2θ = 43.23 and 63.20 refer to the lattice plane (002) and (220) respectively, indicative of Halite structure of MgO (matched JCPDS data card No.61325) confirming the single phase up to 5%. However the samples at higher concentration were exhibited mixed phase as XRD Pattern displayed reflection of MgO of ZnO collectively.

3.2Morphological Analysis

3.2.1 SEM Image of Mg Doped ZnO synthesized by Solid state reaction method

SEM micrographs of Mg doped (1%, 5%) ZnO synthesized by solid state reaction method are shown in the figure 3.8(a) and (b). Well defined grains spherical geometry observed in both the samples. It was noticed that the grains have small size at higher concentration (5%).

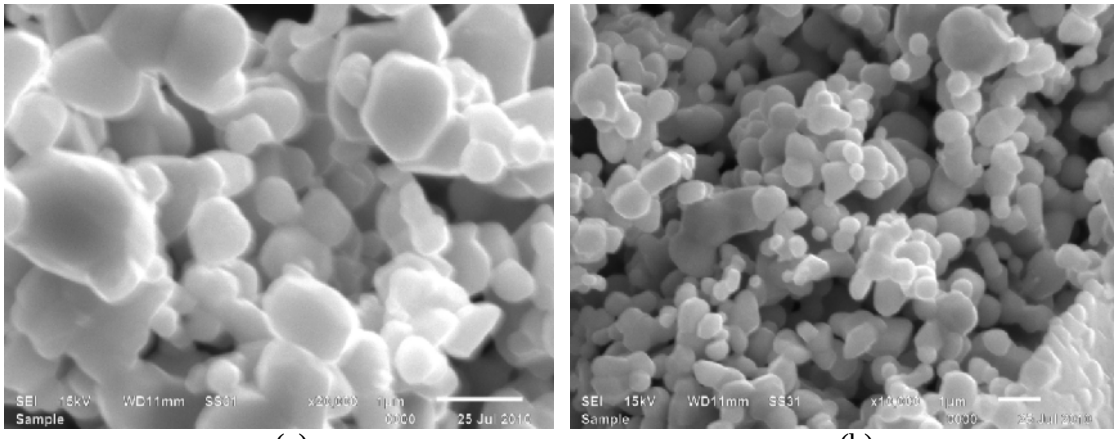

(a) (b)

Fig3.8: SEM image of Mg doped ZnO synthesized by solid state reaction method at 10,000X **(a)** 1%**(b)** 5%

3.2.2 SEM Image of Mg Doped ZnO synthesized by co-precipitation method

3.2.2.1 SEM Image of Mg Doped ZnO synthesized by co-precipitation method in distilled water

SEM micrographs of Mg doped ZnO (5%) synthesized by co-precipitation method in distilled water are shown in the figure 3.9. From the figure it is quite evident that there is no definite morphology in the sample. It seems that the particles were agglomerated and forming a cluster. As the particle size calculated from the XRD is in nano range we are not getting any

exact information from the SEM micrograph, because of the limitation of our instruments up to micro range. The morphology observed in the sample not showing any hard grains which gives an idea the small size of the particle which needs to be characterized by Transmission electron microscopy (TEM) to obtained exact morphology and size of the particles.

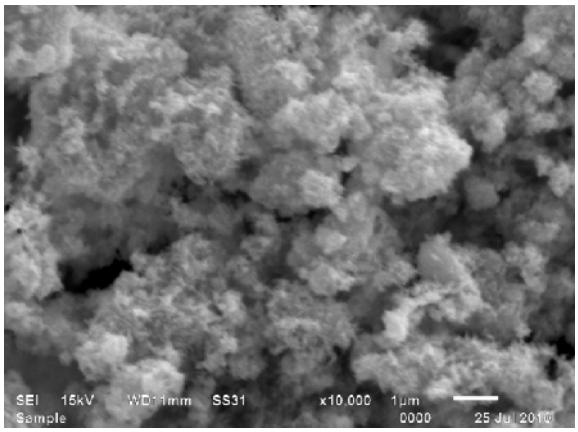

Fig3.9: SEM image of Mg doped ZnO (5%) synthesized by coprecipitaion method in distilled water at 10,000 X

3.2.2.2 SEM Image of Mg Doped ZnO synthesized by co-precipitation method in ethanol

SEM micrographs of Mg doped ZnO (1%, 9%) synthesized by co precipitation method in ethanol are shown in the figure 3.10 (a) and (b). Signature of some spherical particles were obtained from the samples .However it is difficult to distinguished them properly. Size of the particle is small and further needs to be characterized by Transmission electron microscopy (TEM) to obtained exact morphology and size of the particles.

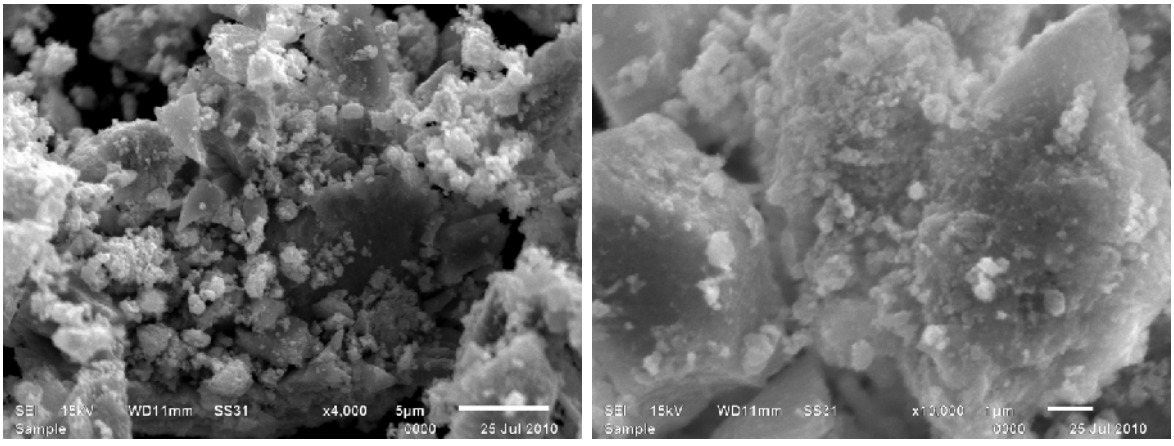

(a) **(b)**

Fig3.10: SEM image of Mg doped ZnO synthesized by coprecipitaion method in ethanol at 10,000 X **(a)** 1% **(b)** 9%

3.2.2.3SEM Image of Mg Doped ZnO synthesized by co - precipitation method in methanol

SEM image of Mg doped ZnO (9%) synthesized by co precipitation method in methanol shown in the figure 3.11 (a) and (b). Some spherical particles were obtained from the samples. However, it is difficult to distinguish them properly.

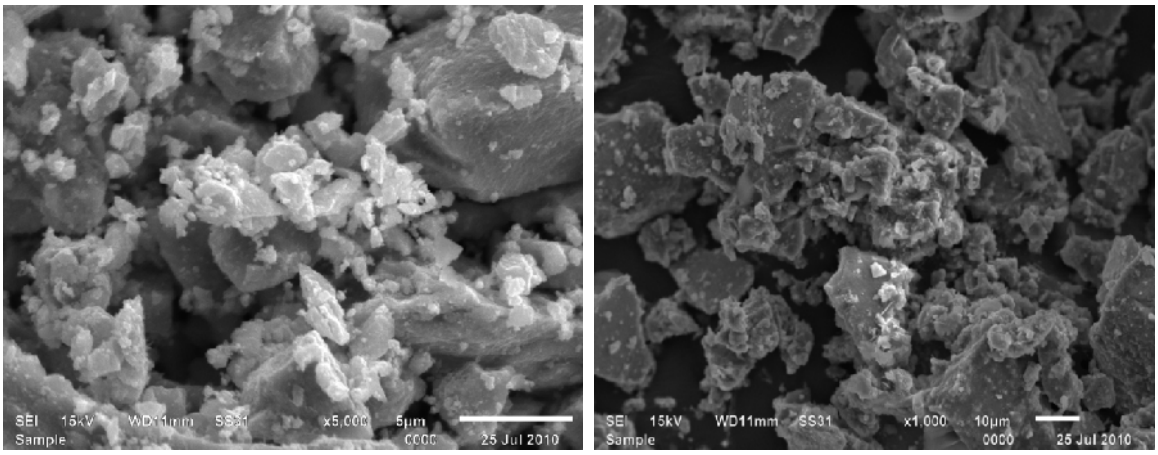

(a) **(b)**

Fig3.11: SEM image of Mg doped ZnO synthesized by coprecipitaion method in methanol at 10,000 X **(a)** ZnO_P **(b)** 9%

3.2.3 SEM Image of Mn Doped ZnO synthesized by co- precipitation method in methanol

SEM micrographs of the synthesized Mn doped ZnO by co precipitation method are shown in the figure 3.12. From the figure it is quite evident that there is less ordered morphology in the sample. It reveals that the particles were agglomerated and forming a cluster

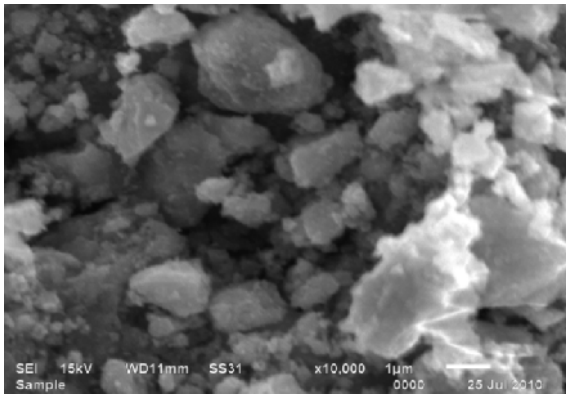

Fig3.12: SEM image of Mn doped ZnO (9%) synthesized by coprecipitaion method in methanol at 10,000 X

3.2.3 SEM Image of Zn Doped MgO synthesized by solid state reaction method

SEM micrographs of Zn doped MgO (1%, 5%) synthesized by Solid state reaction method are shown in the figure 3.13(a) and (b). No definite morphology was found in the samples. It seems that some flakes were agglomerated with each other.

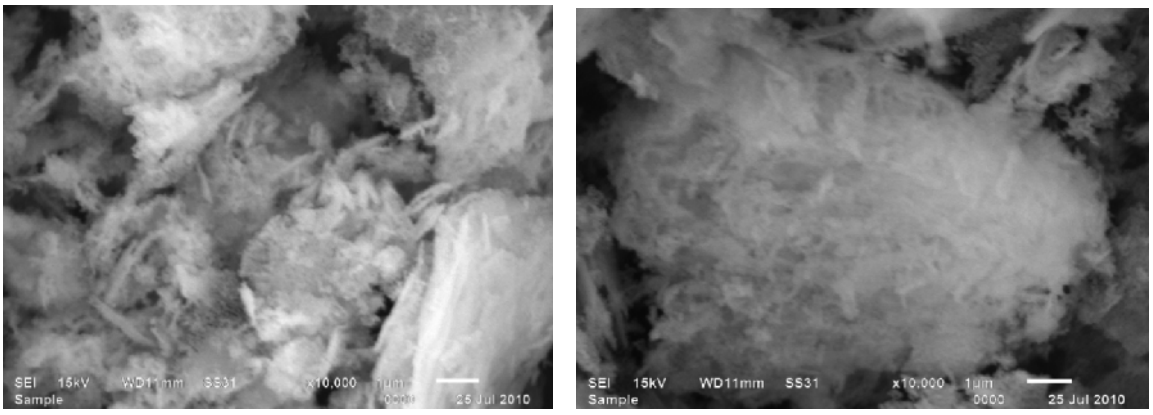

(a) **(b)**

Fig3.13: SEM image of Zn doped MgO (5%) synthesized by solid state reaction at 10,000 X

3.3 Chemical Analysis

3.3.1 FTIR analysis of Mg doped ZnO by co-precipitation method in distilled water and alcoholic medium

Figure 3.14(a),(b) and (c) presenting the FTIR spectrum of Mg doped ZnO synthesized by co-precipitation method in distilled water, ethanol and methanol respectively. Peaks at 1519

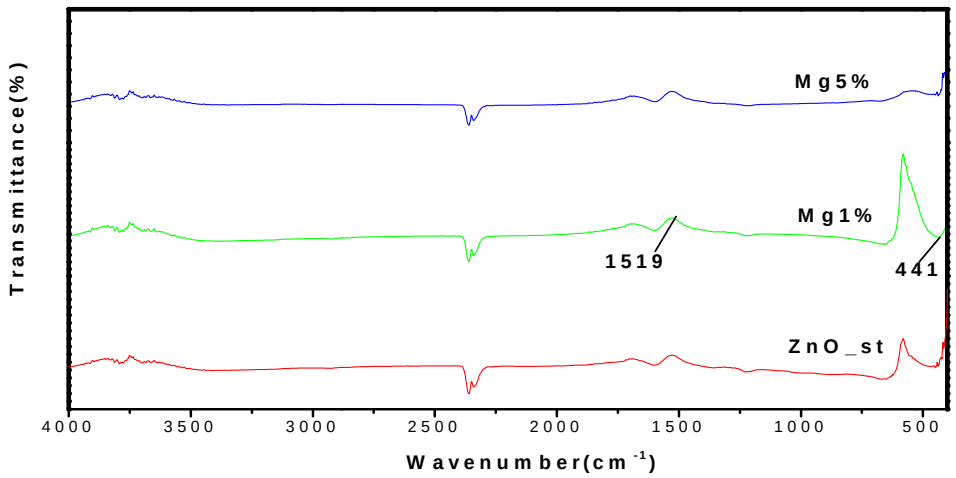

Fig3.14 (a) FTIR spectrum of Mg doped ZnO by co-precipitation method in distilled water

and 441 cm^{-1} corresponds to the COO^- group and Zn-O stretching respectively. However bands at 1476 and 1413 cm^{-1}correspond to MgO were found absent in FTIR spectra which show that there is no unbound content of dopant materials remain in the sample. The dopant was fully fit in the valance site of ZnO.

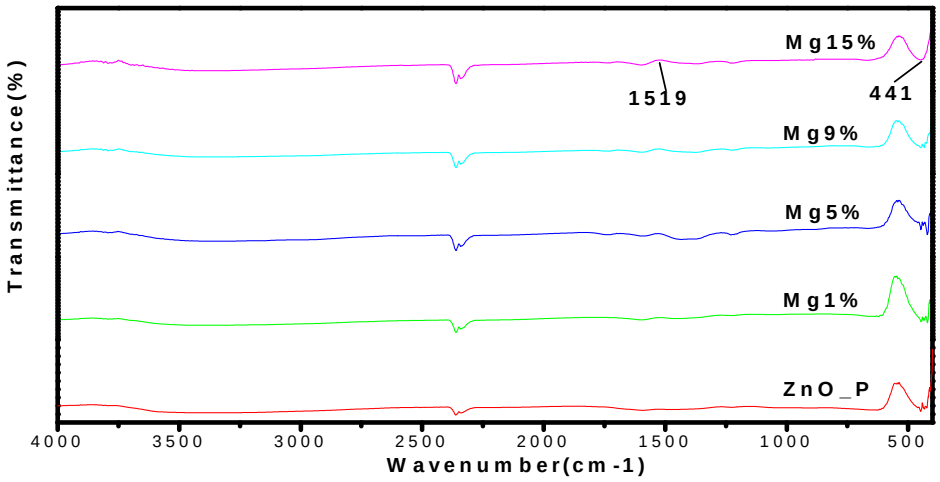

Fig3.14 (b) FTIR spectra of Mg doped ZnO by co-precipitation method in ethanol

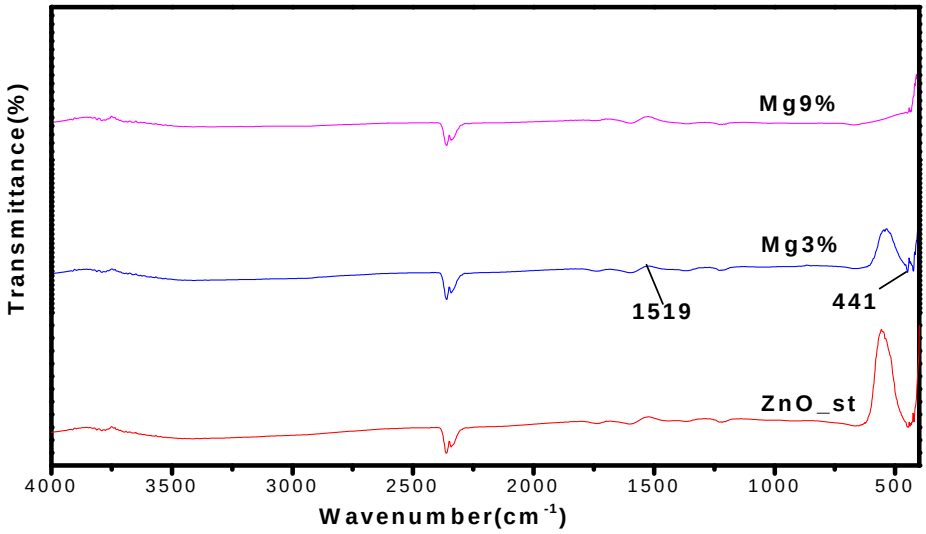

Fig3.14(c) FTIR spectrum of Mg doped ZnO by co-precipitation method in methanol

3.3.2 FTIR analysis of Mg doped ZnO by co-precipitation method in methanol

Figure 3.15 shows the FTIR spectra of Mn doped ZnO (7%, 9%). Peaks observed at 1519cm^{-1} and 441 cm^{-1} corresponds to the COO^- group and Zn-O stretching respectively. It was noticed that Mn content fully doped on the ZnO.

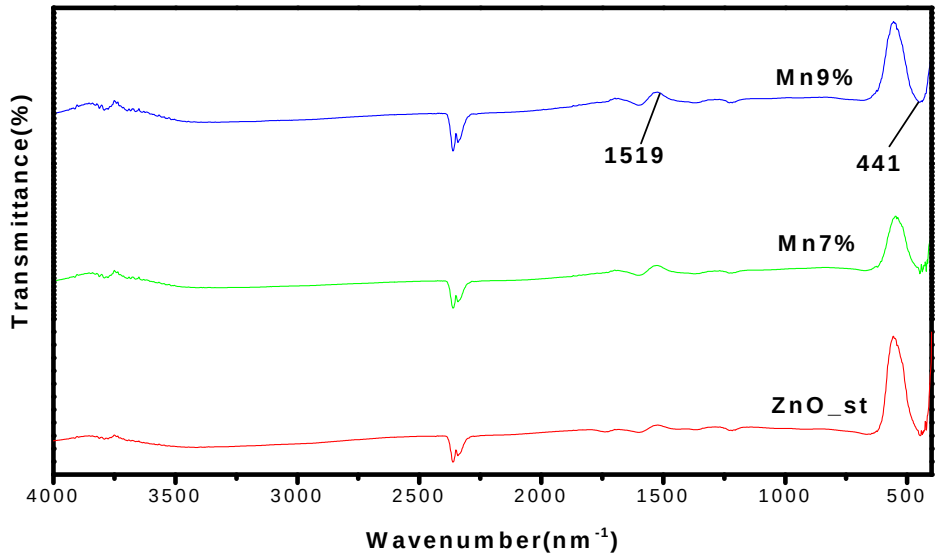

Fig3.15 FTIR spectra of Mn doped ZnO by co-precipitation method in methanol

3.4 Optical characterization

3.4.1 UV-VIS analysis

3.4.1.1 UV- visible analysis of Mg doped ZnO synthesized by solid state reaction method

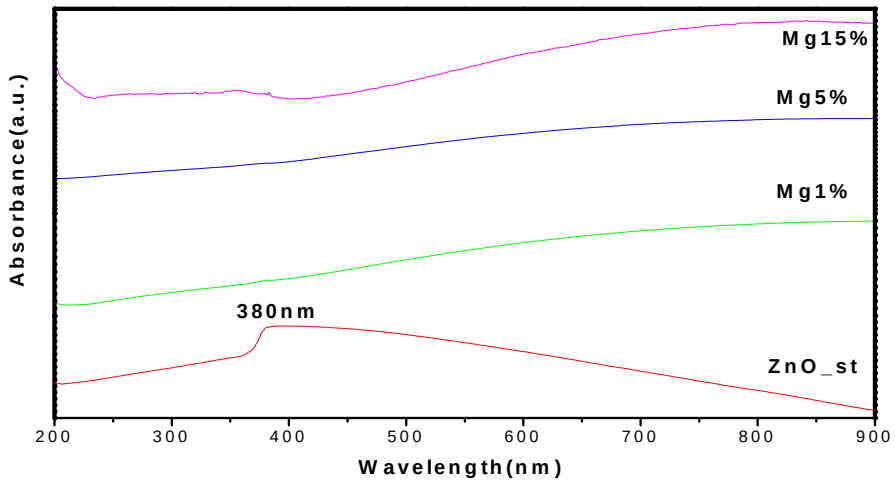

Fig3.16:UV-Visible spectra of Mg doped(1%,5%,15%)ZnO by solid state reaction method

The UV spectrum of Mg doped ZnO synthesized by solid state reaction method is shown in figure3.16. Peak observed for commercially available ZnO at 380nm. There were no characteristic signature of ZnO appeared with dopant at lower and higher concentration.

3.4.1.2.1UV- visible analysis of Mg doped ZnO synthesized by co precipitation method in distilled water

The UV spectrum of Mg doped ZnO (1%, 5%) prepared by co precipitation method are shown in figure3.17. Characteristic peak observed at 380 nm at 1% of Mg doping concentration. The calculated optical band gap for the observed absorption is 3.26eV.

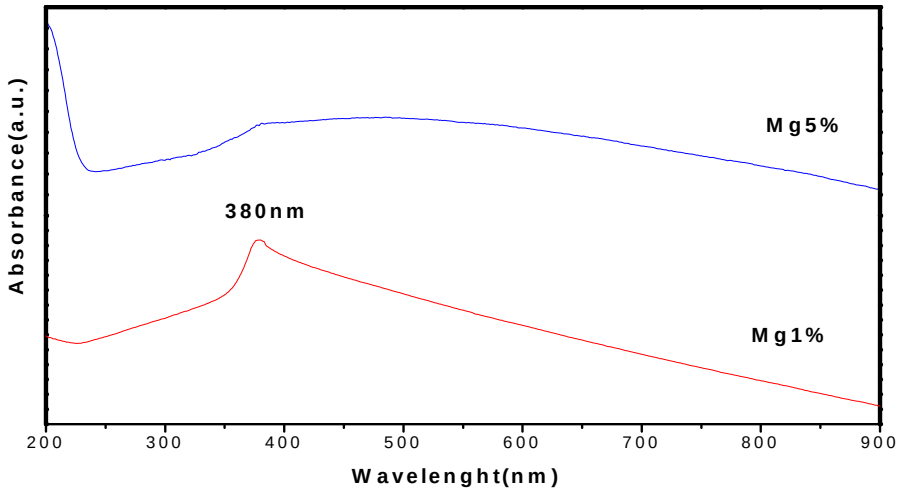

Fig3.17: UV-Visible spectra of Mg doped (3%,9%)ZnO by co precipitation method in distilled water

3.4.1.2.2UV visible analysis of Mg doped ZnO synthesized by co precipitation method in ethanol

The UV spectrums of Mg doped ZnO synthesized by co - precipitation method in ethanol as a solvent are show in figure 3.18. The absorption peak observed at 364 nm in case of pure ZnO, which consequently shift to lower side with increase in dopant concentration. For these absorption peaks optical direct band gap calculated for Mg1%, 9%, 15% is 3.40 eV, 3.44eV, 3.47eV, 3.51eV respectively. In such case the band gap increases as Mg doping concentration increase.

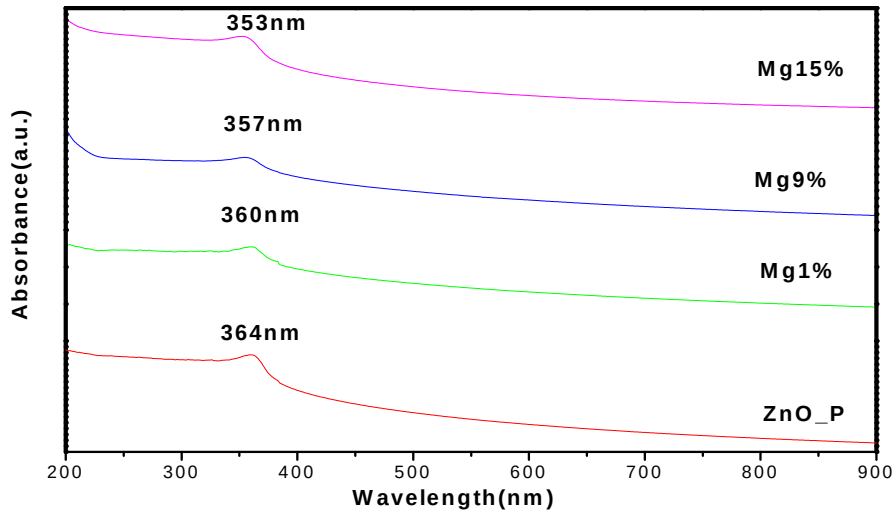

Fig3.18: UV-Visible spectra of Mg doped(1%,9%,15%)ZnO by co precipitation method in ethanol

3.4.1.2.3UV visible analysis of Mg doped ZnO synthesized by co precipitation method in methanol

The UV spectrums of Mg doped ZnO synthesized by co precipitation method in ethanol as a solvent are show in figure 3.19. The absorption peak observed at 370 nm in case of pure ZnO, which consequently shift to lower side with increase in dopant concentration. For these absorption peaks calculated optical direct band gap are 3.35eV, 3.44eV, 3.47eV respectively. In these cases the band gap increases as Mg doping concentration increase.

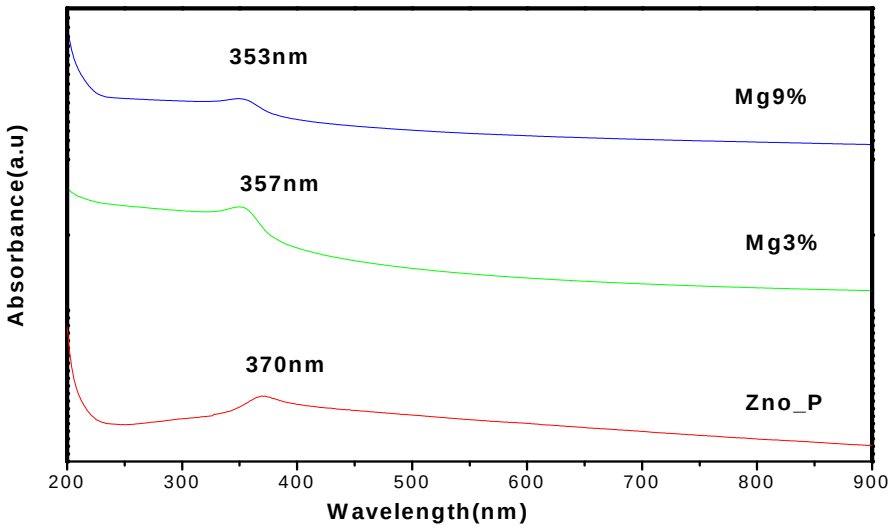

Fig3.19: UV-Visible spectrums of Mg doped(3%,9%)ZnO by co precipitation method in methanol

3.4.1.3UV visible analysis of Mn doped ZnO synthesized by co precipitation method in methanol

The UV spectrums of Mn doped ZnO synthesized by coprecipitaion method are shown in figure 3.20. The peak observed for ZnO at wavelength 370 nm. The optical direct band gap calculated from the standard formula Eg = hc/λ for pure, Mn7% and 9% is 3.35 eV, 3.40eV, 3.44eV respectively.

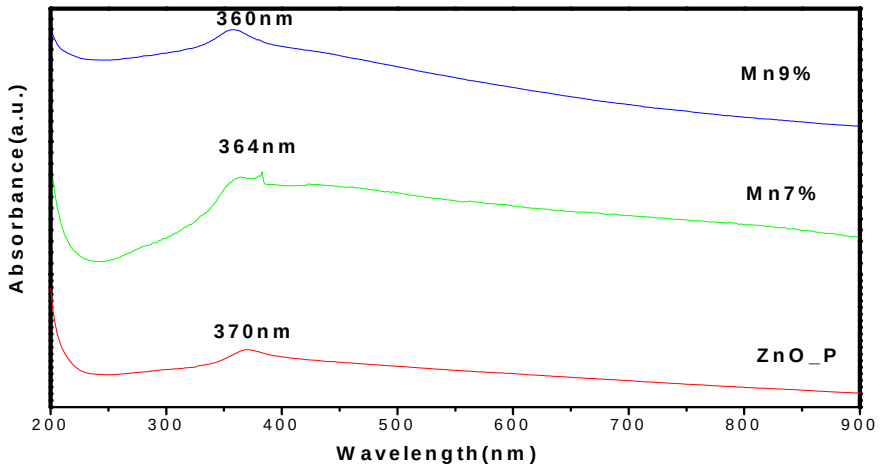

Fig3.20: UV-Visible spectra of Mn doped (7% and 9%) ZnO by co precipitation method in methanol

3.4.1.4 UV- visible analysis of Zn doped MgO synthesized by solid state method

The UV spectrum of Zn doped MgO synthesized by solid state reaction method (firing temperature was 900^0C for 2 hour) shown in figure3.21. No observance peak was found at any concentration.

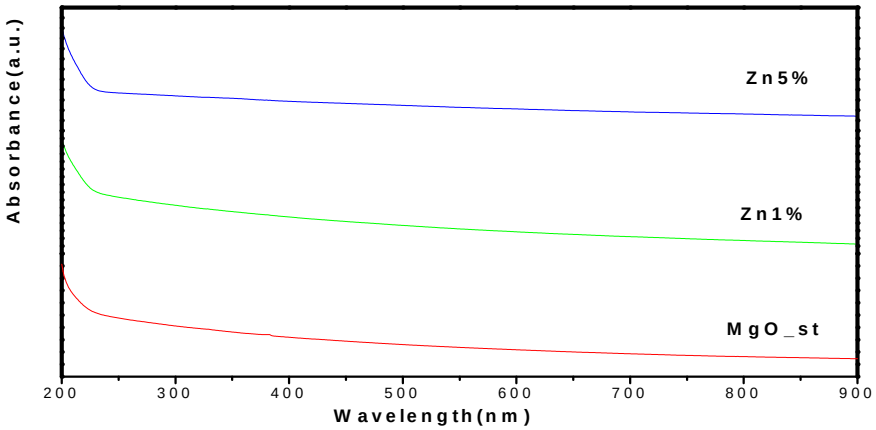

Fig3.21: UV-Visible spectra of Zn doped (1% and 5%) MgO by solid state reaction method

3.4.2 Photoluminescence spectra analysis

The photoluminescence spectra were recorded by spectrofluorophotometer RF-5301PC to find the emission in synthesized samples. Figure 3.22 displayed the excitation spectra of synthesized samples. Two excitation peaks of lower and higher intensity were found at 250nm and 400nm respectively. All the samples were tested at different excitation wavelength (250nm, 360nm, 400nm), we have noticed that the synthesized pure and doped samples shows emission at 250nm excitation wavelength. However there was no emission was scan at 360nm and 400nm excitation wavelength. So we used 250nm excitation wavelength for all further characterization.

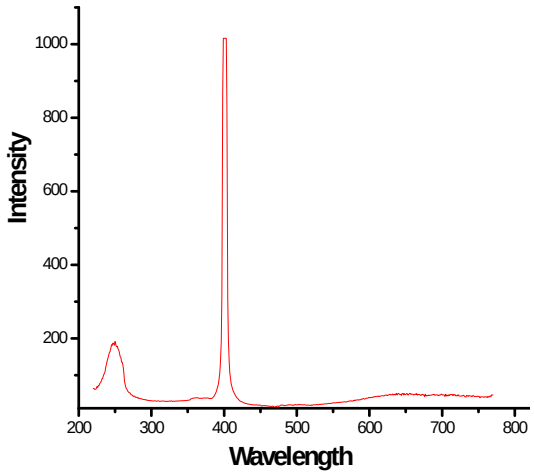

Fig3.22: Excitation spectra of synthesized sample (Mg doped ZnO)

3.4.2.1 Photoluminescence spectra of Mg doped ZnO prepared via solid state reaction

Figure 3.23 displayed the PL spectra of Mg doped ZnO prepared by solid state reaction method. Two characteristic peaks were observed at 400nm and 470nm corresponding to the violet and blue color band. The intensity of the emission peaks were found to increase with increase in the doping of Mg.

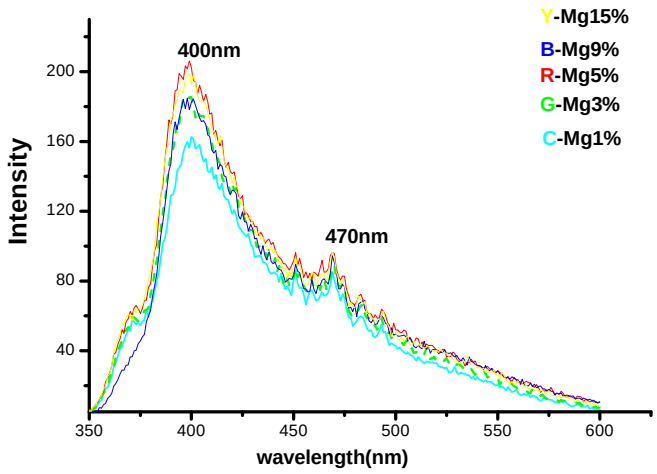

Fig3.23:(a)) Emission spectra of Mg doped ZnO by solid state reaction**(a)** C-ZnO:Mg1%**(b)** G-ZnO:Mg3%g **(c)** R-ZnO:Mg5% **(d)** B-ZnO:Mg9% **(e)** Y-ZnO:Mg15% (Ex-250nm)

3.4.2.2Photoluminescence spectra of Mg doped ZnO by coprecipitaion method in distilled water

Figure 3.24 shows the emission spectra of Mg doped ZnO synthesized using co-precipitation method from distilled water. The PL spectra give emission in complete band of 350nm-600nm. The most intense peaks appeared around 403nm and 470nm were the characteristic of violet and blue colour respectively. The intensity of these emission peaks was found to decrease with doping of Mg.

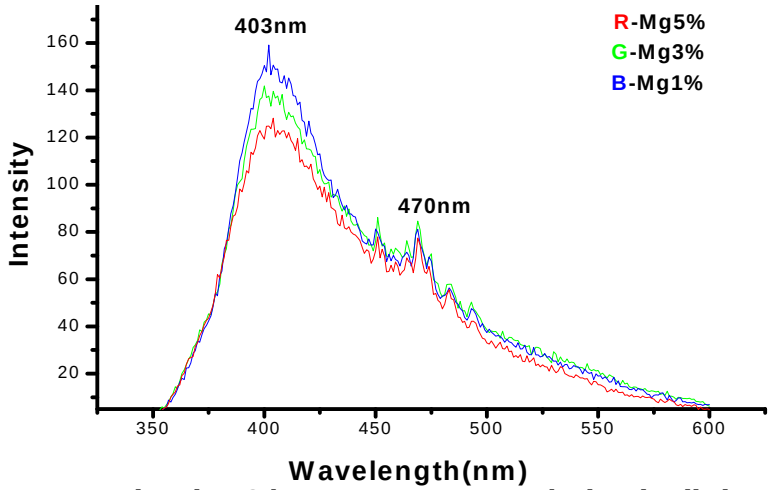

Fig3.24: Emission spectra Mg doped ZnO by co precipitation method in distilled water **(a)** B-ZnO:Mg1%**(b)** G-ZnO:Mg3%g **(c)** R-ZnO:Mg5% (Ex-250nm)

3.4.2.3Photoluminescence spectra of Mg doped ZnO synthesized by co-precipitation method in ethanol and methanol

PL spectra of Mg doped ZnO prepared using co-precipitation method in ethanol and methanol are shown in figure 3.25 and 3.26 respectively. The two characteristics peaks obtained at 400nm and 470nm corresponding to violet and blue colours. The emission was found consistent for methanol based samples. We have noticed that in case of ethanol the intensity of emission peak were found increase upto9% doping concentration of Mg.

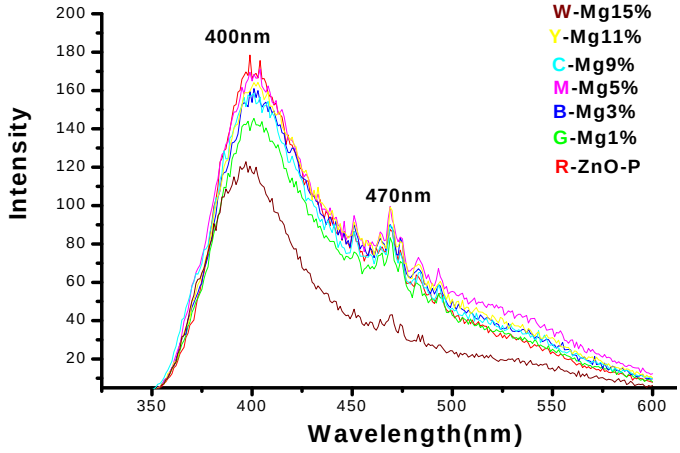

Fig3.25 Emission spectra of Mg doped ZnO by coprecipitaion method in ethanol **(a)**R-ZnO-P**(b)** G-ZnO:Mg1% **(c)** B-ZnO:Mg3% **(d)** M-ZnO:Mg5% **(e)** C-ZnO:Mg9% **(f)** Y-ZnO:Mg11% **(g)**W- ZnO: Mg15% (Ex-250nm).

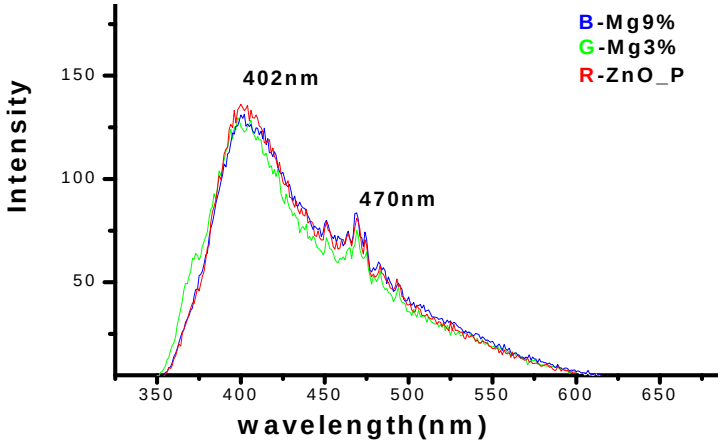

Fig3.26 Emission spectra of Mg doped ZnO by coprecipitaion method in methanol **(a)** R-ZnO_P**(b)**G-ZnO:Mg3% **(c)** B-ZnO:Mg9%(Ext-250)

3.4.2.4Photoluminescence spectra of Mn doped ZnO by coprecipitaion method in methanol

Figure3.27 displayed emission spectra of Mn doped (7% and 9%) ZnO prepared via co precipitation method in methanol. The characteristic emission observed at 394nm indicative of violet colour. From the emission characteristic, we conclude that doping of the Mg and Mn ion only to enhance or reduce the intensity.

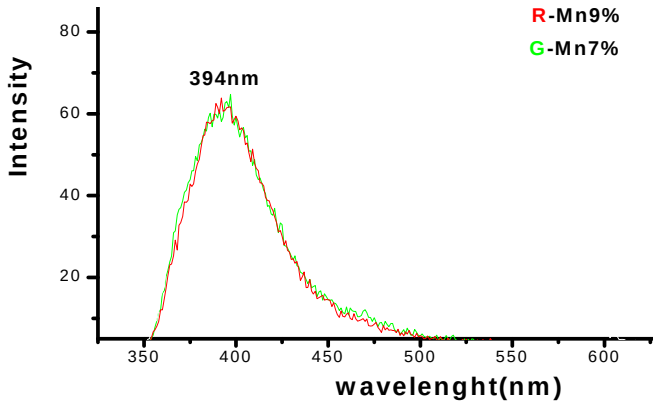

Fig3.27 Emission spectra of Mn doped ZnO **(a)** G-ZnO:Mn7 % **(b)** R-ZnO:Mn9%g (Ex-250nm)

3.4.2.5 Photoluminescence spectra of Zn doped MgO by solid state reaction method

The photoluminescence spectra of Zn doped MgO synthesized by solid state reaction method are shown in figure3.28. The PL spectra give emission in complete band of 350nm-600nm. In this emission band the most intense peak was observed at 368 and 400nm, which corresponds to Violet colour.

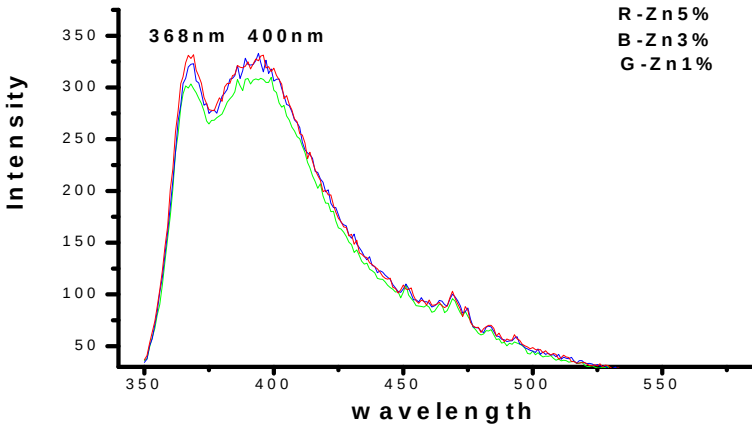

Fig 3.28 Emission spectra of Zn doped MgO by solid state method **(a)** G-MgO: Zn1 % **(b)** B-MgO:Zn3%g **(c)** R-MgO:Zn5% (Ex-250nm)

Chapter 4
Conclusion and Future scope

4.1 Conclusions

1. In summary, we have successfully synthesized Mg and Mn modified ZnO via solid state reaction method and chemical co-precipitation method using various solvent including distilled water, ethanol and methanol.
2. Single phase wurtzite hexagonal structure of ZnO has been achieved up to the higher percentage of dopant (15%) via solid state reaction method at 900^0C. However, single phase of ZnO have been achieved up to the higher percentage of dopant via chemical approach at extremely lower temperatures. The sample prepared via co-precipitation method displayed single phase with smaller size around 300-400 nm in case of ethanol and methanol solvents. Although the doping restrict to 7% in the distilled water case. In addition Zn ion was also successfully doped on the MgO matrix up to 5%.
3. Morphological investigations suggesting the formation of well defined spherical grains in the samples derived from the solid state reaction method. Although no definite morphology was noticed in the doped samples synthesized via chemical route. Only the signature of the some spherical geometries were appeared in these systems, which further needs to be evaluated using TEM.
4. Chemical analysis gives preliminary signature of the ZnO formation in all cases.
5. The UV-Visible analysis inferring that there is no absorption peak found in the samples prepared via solid state reaction method. The well defends absorption shoulder obtained in all the samples derived from the chemical route in three medium. The band gap was found to increase with increment in the dopant concentration as the shift in the absorption peak has been noticed to the lower side.
6. No emission was seen at the excitation wavelength 360 and 400 nm in the PL spectra. However, violet and blue emissions were noticed in all the Mg doped samples at the excitation wavelength 250 nm. It is quite reasonable to say that such materials with enhanced properties can be batter future prospective for many technological applications.

4.2 Future scope

The European Commission has listed ZnO nanopowder as one of the major nonmaterial's anticipated to be intensely commercialized in 2006-2014. Zinc oxide nonmaterial's has attracted hefty research funding due to its highly versatile and promising applications in biotechnology (antibacterial, antifungal, antifouling and biosensors), ultraviolet (UV) applications (catalysis, sunscreen, paint, polymer nano composite and rubber) and opto-electronics (light emitting diodes, field effect transistors, field emitters, solar cells, toners, sensors). Other applications include ZnO used in ferrite, varistor, cement, pigment, ceramic flux, animal food, pollutant filter, dental filling, hydrogen fuel and nano-textile.

Future cars may have ZnO-embedded car seat that can kill microbes, clean on its own and can retard fire. Windows and windscreens can be coated with ZnO nanocomposite layer that repels water, self-cleans and prevents UV penetration. Nanoparticles of ZnO can be added into engine oil to reduce mechanical friction thereby improving fuel-efficiency. Future generation auto engine may be using hydrogen fuel that employs nanoparticles of zinc and ZnO as the media to store and generate hydrogen gas from water.

ZnO light emitting diodes (LEDs) are very promising products that may be used for the head light and it is said they are very efficient and use much less power than bulbs. Finally car paints that incorporate nano ZnO in its recipe are more durable, water repellent and anti-static. The biggest users of ZnO are manufacturers of rubber, followed by smaller applications in paints, coatings, varistors, sunscreens, ferrites, medicated powder, animal food and cements. Currently the mass production of nano ZnO is mainly catered for the sunscreen and cosmetics industries whereby nano ZnO (together with Titania) serves as the UV absorber.

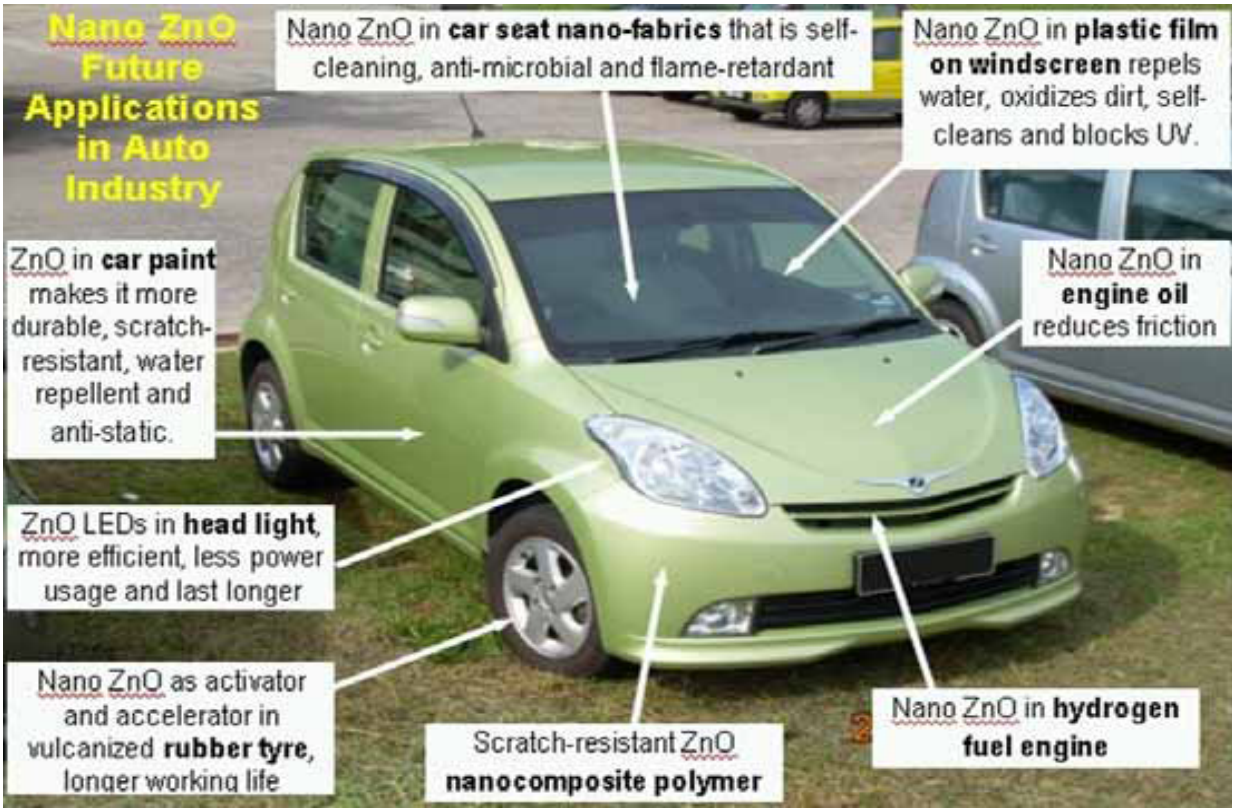

Fig.4.1 Future applications of nano ZnO in the automotive industry

It is expected that by 2015, ZnO nonmaterial's will be mass produced in a much larger tonnage for various applications in automotive catalysis, sunscreens, antibacterial products, rubber vulcanization, fungi statics, pigments, nano-textiles, high-performance coatings, water treatment, dental fillings, hydrogen fuel systems, chemical sensors, pollutant filters, toners, and optoelectronics.

4.3 Proposed Future Research

The study of phosphor provides knowledge and throws light on the use of the materials as a phosphor in display and lighting devices. The study of optical properties will give the applicability of the prepared materials as display device phosphors.

Table2.1 Proposed Future research work

Material	**Doping element**	**Method**	**Process**	**Properties**
ZnS	Mg^{+2},$Mn^{+}2$,Mn^{+4} Cd ,Eu^{+},Fe,Cu,Co etc.	Solid state reaction	Conventional heating	Optical
ZnO	Mn^{+2},Mn^{+4},Cd ,Eu^{+} Etc.	Solid state reaction	Conventional heating	Optical
ZnO	Mn^{+2},Mn^{+4},Cd,Eu^{+} etc.	Sol –gel method	Perception	Optical
ZnO	Mn^{+2},Mn^{+4},Cd,Eu^{+} etc.	Sol –gel method in presence of LiOH, KOH etc.	Perception	Optical
MgO	Mn^{+2},Mn^{+4},Cd,Eu^{+} etc.	Sol –gel method	Perception	Optical

References

[1] W.H. Suh, K.S. Suslick, G.D. Stucky, Y.H. Suh; Nanotechnology, **87**, 70(2009)

[2] K. X. Yao, R. Sinclair and H.C. Zeng; Journal of Physical Chemistry, **11**, 2032(2007)

[3] B.A.Korgel and D. Fotzmaurice; Advance Materials, **10**,661(1998)

[4] W.Q. Peng, G.W.Cong, S.C. Qu, Z.G.Wang; Optical material, **29**,313(2006)

[5] C. Bouvy, F.Piret, W.Marine, B.L.Su; Chemistry Physical Latter, **433**,350(2007)

[6] M. Faraday; Phil. Trans. Roy. Society. London **147**,145(1857)

[7] G.T. Beilby; Proc. Royal Society. A **72**,226(1903)

[8] T. Turner; Proc. Royal Society London, A **81**, 548,301 (1908)

[9] P. Buffat, J.P. Burrel; Physical Review A **13** (6), 2287(1976)

[10] C.W. Bunn; Proc. Phys. Soc. London, **47**, 835 (1935)

[11] M. Willander, O.Nur, Q.X Zhao, L.L.Yang, M. Lorenz, B.Q Cao, J. Zuniga Perez, C. Czekalla, G. Zimmermann, M. Grundmann, A.Bakin, A. Behrends, M. Al-Suleiman, A. Al-Shaer, A. Che, B. MoforPostels, A.Waag, N. Boukos, A. Travlos, H.S. Kwack, J. Guinard, D.Le Si Dang; Nanotechnology, **20**, 332001(2009)

[12] H.A. Ahn, Y.Y. Kim, D.C. Kim, S.K. Mohanta, H.K. Cho ; Journal of Applied Physics, **105**, 013502 (2009)

[13] W. Liu, L.S.Gu, D.L .Ye., S.M. Zhu, S.M. LiuZhou, R. Zhang, Y. Shi, Y. Hang ,C.L. Zhang; Applied Physical Letter., **88**, 092101 (2006)

[14] P.X.Gao, Y.Ding, Z.L. Wang; Nanotechnology Letter, **3**, 1315(2003)

[15] C. Klingshirn; Physical Stat. Sol. B, **244**, 3027(2007)

[16] C.Klingshirn, E. Mollwo; Zeitschrift fur Physik A, **254**, 437(1972)

[17] J. J. Lander; Journal of Physical Chemistry, **15**, 324(1960).

[18] D. Zwingel; Journal of Luminescence, **5**, 385(1972)

[19] D.C. Look, B. Claflin; Phys. Stat. Sol. B, **241**, 624(2004)

[20] Ü. Özgür, Ya.I. Alivov, C.Liu, A. Teke, M.A. Reshchikov, S. Dogan, A. Avrutin S-J.Cho, H. Morkoç; Journal of Applied Physics, **98**, 041301, 103(2005)

[21] P.X. Gao, Z.L.Wang; Small, **1**,945(2005)

[22] M.L. Fuller; Journal of Applied Physics, **15**, 164 (1944)

[23] Z.L. Wang, Journal of Applied Physics, A **88**, 7 (2007)

[24] B.G.streetman, Solid state electronic devices 5th ED, (2000)

[25] U .Ozgur, Journal of Applied physics, **98,** 41301(2005)

[26] M. Grätzel, Photo electrochemical cells, Nature **414**, 338(2001)

[27] S. Singh ,P. Thiyagarajan, K .Mohan Kant ,D. Anita, S. Thirupathiah, N. Rama, B. Tiwari,M. Kottaisamy and M. S. Ramachandra Rao; Journal of Physics. D: Appl. Phys. **40 ,**6312(2007)

[28] R. Chaudhary; M.Tech Thesis, thapar.edu (2009)

[29] D. C. Look, J. W. Hemsky, J. R. Sizelove, Physical Review Letters,**82**, 12 (1999)

[30] O. Zgur, X. Gu, S. Chevtchenko, J. Spradlin,J. Cho,H. morkocx, F.H. Pollak, H.O. everitt and J.E. Nause , Journal of Electronic Materials, **35**, 4, (2006)

[31] T. Olorunyolemi, A. Birnboim, Y. Carmel, O. C. Wilson and I. K. Lloyd, Journal of Am. Ceramic. Soc. **85**, 1249 (2002)

[32] B.K. Meyer; Physics. Stat. Sol. (B) **241**, 231 (2004)

[33] A. Janotti, C.G. Van de Walle; Physical Rev. B, **76,** 16520(2007).

[34] C.G. van de Walle; J. Neugebauer; Journal Applied Physics, **95**, 3851(2004)

[36] P.M. Mooney, Academic Press: San Diego, CA, USA, B, **51**, 93

[37] D.C. Look; J.W. Hemsky; J.R. Sizelove; Phys. Rev. Lett., **82**, 2552(1999)

[38] F.A. Kröger, North Holland press: Amsterdam, The Netherland, (1964)

[39] F. Tuomisto, K. Saarinen, D.C. Look , G.C. Farlow; Phys. Rev. B, **72**, 085206(2005)

[40] Tuomisto, F.; Saarinen, K.; Look, D.C.; Phys. Stat. Sol. C, **201**, 2219(2004)

[41] D.C. Look, G.C. Farlow, P. Reunchan, S. Limpijumnong, S.B.Zhang, K. Nordlund; Physical Review Letter, **95**, 225502(2005)

[42] F.A. Kröger, H.J. Vink, Journal of Applied Chemistry Phys., **22**, 250(1954)

[43] A.F. Kohan, G. Ceder, D. Morgan, C.G. F. Van de Walle, Physical Review, B, **22**, 15019(2000)

[44] F. Oba, S.R. Nishitani, S. Isotani; H. Adachi, I. Tanaka; Journal of Applied Physics, **90**, 824(2001)

[45] A.B. Djurisic, Y.H. Leung, K.H. Tam, L. Ding, W.K. Ge., H.Y. Chen., Applied Physical Letter, **88**, 103107(2006)

[46] S.A.M. Lima, F.A. Sigoli, M. Jafelicci, M.R. Davolos; Int. Journal Inorganic Mater, **3**, 749. (2001)

[47] B. Lin, Z. Fu, Y. Jia; Applied Physical Letter, **79**, 943(2001)

[48] V. Nikitenko; Springer: Dordrecht, The Netherland, **69**(2005)

[49] C.G. van de Walle, Physical. Review Letter, **85**, 1012(2000)

[50] O.F. Schirmer; D. Zwingel; Solid State Commun., **8**,1559(1970)

[51] D.P.Norton, Y.W.Heo, M.P.Ivill; Mater Today, **7, 34**(2004)

[52] K.L.Chopra, S. Major, D.K. Pandya; Thin solid film, **102**,(1983)

[53] N.J.Dayan, S.R. Sainkar; R.N. Karekar; Thin solid film, **325,254**(1998)

[54] G.Kiriakidis and N.Katsarakis; Journal of Physics Condense Matter,**16**, 3757(2004)

[55] R.C. Wang, C.P. Liu, J.L.Huang, Applied Physics Letter,**87**, 013110(2005)

[56] A.R.West, Solid State Chemistry, John Wiley & Sons, 1987

[57] A.Ohtomo,M.Kawasaki,T.koida,K.Masubuchi,H.Koinuma,Y.Sakurai,Y.Yoshida,T.Yasud,H.M.Jang; Applied Physical Letter,**72**,2466(1998)

[58] W.I.Park, Gyu-chul Yi, H.M. Jang; Applied Physics Letter, **72**, 2022(2001)

[59] S.Choopun, R.D. Vispute, W.Yang, R.P.Sharma; Applied Physics Letter,**80**, 1529(2002)

[60] J. Narayan, A.K.Sharma, A. Kvit, C. Jin, J.F.Muth.O.W.Holland; Solid State Commun. **121**,9(2002)

[61] A.N.Baranov,V.L.Solozhenko,C.Chateau,G.Bocquillon,J.P.Petitet,G.N.Panin,T.W.Kang, RV. Shpanchenko, E.V.Antipov, Y.J.Oh; Journal of Physics: Condense Matter, **17**, 3377(2005)

[62] S.Sundar Manoharan, S.Arora, Material Science and Engineering ,**162**,68(2009)

[63] S. Shionoya and W.M. Yen, Phosphor Handbook(Boca Raton, FL: CRC Press) ,**565**(1999)

[64] B. Lin, Z. Fu and Y. Jia ;Applied Physics Letter ,**79** ,943(2001)

[65] M. Liu, A. H. Kitai and P. Mascher ; Journal Luminescence,**54** ,35(1992)

[66] Z. Fang; Y. Wang; D. Xu; Y. Tan and X. Liu, Optical Material,**26** ,42(2004)

[67] V. Z. Mordkovich, H. Hayashi, M. Haemori, T. Fukumura and M .Kawasaki; Advance Functional Material, **13**, 24(2003)

[68] Y.S.Wang, P.John Thomas; Journal of Physical Chemistry,**110**,214159(2006)

[69] H. Q. Li, Q Wan, Y.G. Wang; Applied Physical Letter, **86**, 263101(2005)

[70] M. Lorenz, E. M. Kaidashev, A. Rahm, T.Nobis, J.Lenzner; Applied Physical Letter, **86**, 133107(2005)

[71] A. Waag, C.kirchner,T. Gruber,R. Reuss and R. Kling; Physical Status solid(2007)

[72] J. Lim, K. Shin, H.W.Kim and C Lee; Journal of Luminescence, **109**, 5(2004)

[73] J. Jhang, Z. Zhang and T. Wang; Chemical Material,**16**, 70(2004)

[74] L. Bergman, J. L. Morrison, Chen X-B; Applied Physics, **39**, 42(2006)

[75] S. Kumar Senthil, K.Rajendran, S.Banerjee, T.K.Chini, V.Sengodan; Materials Science in Semiconductor Processing, **11**, 6 (2008)

[76] R. Vidya Sagar, S. Buddhudu ; Physics Letters A, **373**, 3184(2009)

[77] M. Godlewski , A. Wojcik-Głodowska E. Guziewicz ,S. Yatsunenko ,A. Zakrzewski

Y. Dumont, E. Chikoidze, M.R. Phillips; Optical Materials, **31** ,1768 (2009)

[78] N. Ohashi; NNIN REU Research Accomplishments, 150(2008)

[79] S.R. Dhage and V. Ravi; Materials Letter, **59**, 779(2005)

[80] M. Nicholes and K.Drake; Journal of Alloy & Compound, **312**, 30(2000)